

Doctoral Dissertation (Censored)

博士論文 (要約)

Studies on the relationship of mitochondrial RNA processing to cell division control underlying
early development of lateral roots in Arabidopsis

(シロイヌナズナの側根形成初期における細胞分裂制御とミトコンドリア RNA
プロセッシングの関係性についての研究)

A Dissertation Submitted for the Degree of Doctor of Philosophy

July 2020

令和 2 年 7 月博士 (理学) 申請

Department of Biological Sciences, Graduate School of Science,

The University of Tokyo

東京大学理学系研究科

生物科学専攻

Akihito Mamiya

間宮章仁

Table of contents

Abstract	2
Acknowledgements	3
List of abbreviations	4
Chapter 1. Introduction	6
Chapter 2. Results	12
Chapter 3. Discussion	19
Chapter 4. Materials and Methods	25
Chapter 5. References	31
Figures and tables	39

Abstract

Although mechanisms that activate organogenesis in plants are well established, much less is known about the subsequent fine-tuning of cell proliferation, which is crucial for creating properly structured and sized organs. In this thesis, I studied the formation of lateral roots (LRs) in *Arabidopsis* as a model of plant organogenesis with a focus on the control of cell division during its early stages. In particular, I analyzed three temperature-dependent fasciation (TDF) mutants of *Arabidopsis*, *root redifferentiation defective 1* (*rrd1*), *rrd2*, and *root initiation defective 4* (*rid4*), which are characterized by the formation of abnormally broadened (i.e., fasciated) LRs under high-temperature conditions due to excessive cell division. Previous studies have revealed that all TDF genes encode putative RNA processing factors that show mitochondrial localization and that phenocopy of the TDF phenotype is achieved by chemical inhibition of mitochondrial respiration. These results raised the possibility that the TDF mutations cause an impairment of the mitochondrial respiration, which in turn leads to excessive cell proliferation during early LR development via an unknown mechanism. However, the exact functions of the TDF proteins had not been elucidated. Moreover, the molecular mechanisms that connect mitochondrial respiration to the control of cell division in LR organogenesis remained totally unknown. In this thesis, I first demonstrate that *RRD1*, which encodes a poly(A)-specific ribonuclease (PARN)-like protein, participates in the removal of poly(A) tails from transcripts of most mitochondrial genes. I also demonstrate that *RRD2* and *RID4*, both of which encode a PLS-class pentatricopeptide repeat (PPR) protein, target specific mitochondrial mRNA for site-directed C-to-U RNA editing. I further reveal that all TDF mutants carry defects in the biosynthesis of the electron transport chain. *rrd1* and *rrd2* show decreased cytochrome *c* (*cyt c*) levels at high temperature, whereas *rid4* shows a dramatic reduction in complex V (ATP synthase) levels regardless of temperature conditions. The observed influence of *rrd1* on *cyt c* levels also leads to the discovery of a relationship between the poly(A) status and RNA editing levels in *cytochrome c biogenesis factor 3* (*ccb3*) mRNA. By performing pharmacological analysis, I also show that the generation of reactive oxygen species (ROS) might be a trigger of excessive cell division in the TDF mutants. Finally, I discuss possible mechanisms of ROS-induced LR fasciation. Together, my study provides novel insights into the molecular machinery involved in mitochondrial RNA processing and their relationship to cell division control in plants.

Acknowledgements

Firstly, I want to share my extreme gratitude and appreciation to my supervisor Dr. Munetaka Sugiyama for providing great advice and support throughout this study, especially when it mattered the most. I wish to express my deep appreciation to Dr. Sugiyama and former members of his laboratory who paved the way for this study: Dr. Mineko Konishi identified *RID4* by positional cloning, Dr. Atsuko Kinoshita conducted chromosome mapping of *rrd1* and some of the initial characterization of the TDF phenotype, Dr. Hiroaki Tamaki isolated the *rid4-2* mutant, Mr. Masaki Arita and Dr. Masato Saito conducted chromosome mapping of *rid4-2*; Dr. Kurataka Otsuka performed chromosome mapping of *RRD1* and *RRD2*, construction of the reporter genes, subcellular localization analysis of the TDF proteins, microarray data collection, initial analysis of the poly(A) status of mitochondrial mRNAs, and initial pharmacological analysis with respiratory inhibitors; Ms. Kayoko Yamamoto collected preliminary data on the genetic relationship between *rrd1* and *ags1* and performed preliminary analysis of RNA editing; Dr. Mamoru Nozaki designed and performed analysis of PARN activity of recombinant RRD1 and performed preliminary analysis of extracted mitochondrial protein. I wish to thank Drs. Takushi Hachiya and Ko Noguchi for supporting the analysis of the mitochondrial respiratory chain, Dr. Takashi Hirayama for his insightful comments and support on the analysis of mitochondrial mRNA metabolism, and Drs. Takehito Kobayashi, Yusuke Yagi, and Takahiro Nakamura for preliminary analysis and invaluable discussions on mitochondrial mRNA editing. Additionally, I thank Dr. Shin-ichi Arimura for providing the *35S::Mt-GFP* line, Dr. Takashi Hirayama for providing the *ags1* line, Mr. Yuta Otsuka and Dr. Yuki Kondo for the assistance on GFP imaging, Ms. Hatsune Morinaka for the assistance on qRT-PCR, and Dr. Malcolm Bennett for providing the *pAUX1::AUX1-YFP* line, Dr. Daniel von Wangenheim for guidance on light-sheet imaging, and Dr. Takeda Hiroyuki and members of his lab for the assistance on light-sheet imaging. I am also grateful to my examination committee, Dr. Hirokazu Tsukaya, Dr. Yuichiro Watanabe, Dr. Ichiro Terashima, and Dr. Tetsuya Higashiyama, for taking time to read and provide helpful feedback on this thesis. I am thankful for the financial support I received from the Ministry of Education, Culture, Sports, Science and Technology, Japan (MEXT; Graduate Program for Leaders in Life Innovation (GPLLI) at the University of Tokyo Life Innovation Leading Graduate School) and from the Japan Society for the Promotion of Science (JSPS; Grants-in-Aid for JSPS Fellows No. 17J05722)

List of abbreviations

a.a.	amino acid
ABA	abscisic acid
ABC	ATP-binding cassette
<i>ags1</i>	<i>ahg2-1 suppressor 1</i>
<i>ahg2</i>	ABA hypersensitive germination
Arabidopsis	<i>Arabidopsis thaliana</i>
ARF	auxin response factor
ATP	adenosine triphosphate
AUX1	AUXIN RESISTANT 1
BN-PAGE	blue native-PAGE
CAPS	cleaved amplified polymorphic sequences
<i>ccb</i>	<i>cytochrome c biogenesis protein</i>
CCCP	carbonylcyamide m-chlorophenyl-hydrazone
cDNA	complementary DNA
CIM	callus-inducing medium
Col	Columbia
<i>cox</i>	<i>cytochrome oxidase subunit</i>
CR-RT PCR	circularized RNA-RT PCR
<i>cwm2</i>	<i>cell wall maintainer 2</i>
cyt c	cytochrome <i>c</i>
dCAPS	derived CAPS
2,4-D	2,4-dichlorophenoxyacetic acid
DR5	direct repeat 5
EDTA	ethylenediaminetetraacetic acid
GFP	green fluorescent protein
GMA	germination medium solidified with agar
GUS	β -glucuronidase
IAA	indole-3-acetic acid
IBA	3-indolebutyric acid
<i>Ler</i>	Landsberg <i>erecta</i>

LR	lateral root
MES	2-morpholinoethanesulfonic acid
mRNA	messenger RNA
mtPNPase	mitochondrial polynucleotide phosphorylase
<i>nad</i>	<i>NADH dehydrogenase subunit</i>
NADH	nicotinamide adenine dinucleotide + hydrogen
NPA	naphthylphthalamic acid
PAGE	polyacrylamide gel electrophoresis
PAP	poly(A) polymerase
PARN	poly(A)-specific ribonuclease
PAT assay	poly(A) test assay
PCR	polymerase chain reaction
PPR	pentatricopeptide repeat
PQ	paraquat
qRT-PCR	quantitative reverse transcription-PCR
RACE-PAT	poly(A) test assay by rapid amplification of cDNA ends
<i>rid4</i>	<i>root initiation defective4</i>
RIM	root-inducing medium
ROS	reactive oxygen species
<i>rrd1</i>	<i>root redifferentiation defective 1</i>
<i>rrd2</i>	<i>root redifferentiation defective 2</i>
RT-PCR	reverse transcription-PCR
TDF	temperature-dependent fasciation
tRNA	transfer RNA
<i>TUB4</i>	<i>β-TUBULIN4</i>
WT	wild type
YFP	yellow fluorescent protein

Chapter 1. Introduction

Plants elaborate their architecture by continuously developing new organs, such as leaves, floral organs, axillary stems, and lateral roots (LRs). Organogenesis begins with the local activation of cell proliferation in the plant body. In the following stages, proliferation is restricted to certain areas, which is essential for the formation of properly sized and structured organs. However, the molecular underpinnings of such regulation remain mostly unknown.

Arabidopsis LR development as a model for plant organogenesis

LRs serve as building blocks of the root system architecture, and are crucial for the uptake and transport of water and minerals. The first visible step of LR formation occurs within the parental root, where a few cells start to divide, comprising the LR primordium. The LR primordium grows and eventually emerges out of the parental root to form a new LR (Torres-Martínez et al., 2019). This process has been described in detail in the model plant *Arabidopsis thaliana* (Arabidopsis), rendering it one of the most ideal systems to study the molecular mechanisms of organ development (Goh et al., 2016; von Wangenheim et al., 2016). In Arabidopsis, a small number of cells in a few adjacent files of the xylem pole pericycle layer, termed LR founder cells, undergo radial expansion and subsequently re-enter the cell cycle (Ramakrishna et al., 2019; Vermeer et al., 2014; von Wangenheim et al., 2016). They first divide in the anticlinal (perpendicular to the parental root axis) orientation, producing an array of short cells flanked by longer cells, which serve as the origin of the LR primordium (stage I; Fig. 1) (Goh et al., 2016; Malamy and Benfey, 1997; von Wangenheim et al., 2016). This is followed by periclinal (parallel to the surface of the root) divisions throughout the primordium, with the exception of the flanking cells in some occasions, creating two cell layers (stage II; Fig. 1). Subsequent periclinal cell divisions take place in the central zone of the primordium, producing the third cell layer (stage III), followed by the fourth cell layer (stage IV; Fig.1). Additional anticlinal cell division, together with cell expansion at the innermost cell layer, gives rise to a dome-shaped primordium (stage V; Fig. 1).

The local accumulation of the phytohormone auxin is critical for LR initiation, driving LR founder cell identity acquisition and division via the degradation of the SOLITARY ROOT (SLR/IAA14) repressor, thus activating the expression of down-stream genes mediated by the AUXIN RESPONSE FACTORS ARF7 and ARF19 (Lavenus et al., 2013).

Several members of LATERAL ORGAN BOUNDARIES-DOMAIN/ASYMMETRIC LEAVES2-LIKE (LBD/ ASL) family of transcription factors, including LBD16/ASL18 (Goh et al., 2012), LBD18/ASL20 (Berckmans et al., 2011; Lee et al., 2009), and LBD33/ASL24 (Berckmans et al., 2011) are among the direct targets of ARF7 and ARF19 that positively regulate LR initiation (Lavenus et al., 2013; Okushima et al., 2007). LBD18/ASL20 and LBD33/ASL24 activate the cell cycle through the induction of the transcription factor E2Fa (Berckmans et al., 2011). LBD16 functions in the acquisition of centripetal polarity of the LR founder cells prior to stage I (Goh et al., 2012).

Although the mechanisms that activate the first anticlinal cell divisions during LR initiation have been extensively studied, much less is understood about the coordinated periclinal and anticlinal divisions that subsequently take place. In particular, the manner in which cell proliferation becomes confined to the central zone of the primordium, giving rise to the dome-shaped structure, largely remains a mystery (Torres-Martínez et al., 2019), although the requirement of several factors have been shown. One such factor is polar auxin transport (Benková et al., 2003; Geldner et al., 2004). Visualization of auxin response by the Direct repeat 5 (DR5) reporter have shown that during early LR development, a centripetal gradient is formed, in which the signal is maximal at central region of the primordium (Benková et al., 2003). Perturbations of polar auxin transport by mutating multiple PIN-formed (PIN) auxin efflux carriers (*pin1 pin3 pin4*, *pin1 pin4 pin7*, and *pin1 pin3 pin7* (Benková et al., 2003)) or by mutating GNOM, a guanine nucleotide-exchange protein for ADP-ribosylation factor (ARF-GEF) involved in the membrane trafficking of the PIN proteins (Geldner et al., 2004), result in homogeneous proliferation of the pericycle cell layer in large regions of the root upon exogenous auxin treatment, indicating that the formation of the auxin gradient is necessary for limiting cell division during LR development. In addition, the involvement of the spatial control of BODENLOS (BDL)/IAA12-MONOPTEROS (MP)/ARF5-mediated auxin response (De Smet et al., 2010), peptide-receptor interactions (ACR4 receptor (De Smet et al., 2008); RALFL34 peptide (Murphy et al., 2016); GLV6/RGF8/CLEL2 peptide (Fernandez et al., 2015)), transcription factors (PUCHI (Hirota et al., 2007); PLETHORA3, PLETHORA5, and PLETHORA7 (Du and Scheres, 2017)), a H3K4-histone methyltransferase (ARABIDOPSIS HOMOLOG of TRITHORAX1 (ATX1/SDG27) (Napsucialy-Mendivil et al., 2014)), the regulation of symplastic intercellular connectivity by plasmodesmal-localized β -1,3 glucanases (PdBGs) PdBG1 and

PdBG2 (Benitez-Alfonso et al., 2013), and mechanical interaction with the overlaying endodermal tissue (Vermeer et al., 2014) have been implicated in patterning of the division of the pericycle cells during LR initiation.

The unknown roles of mitochondrial gene expression in plant organ development

Plant cells have gene expression systems in mitochondria and plastids in addition to the nucleus. Although organelle gene expression is typically associated with organelle-specific functions, it might also be involved in higher-order physiological activities including the regulation of organogenesis. Mitochondria are considered the “powerhouses” of the cell, as they supply the energy that is necessary for cellular activities. In comparison with other eukaryotes, RNA metabolism in mitochondria is particularly complex in plants, and entails numerous nuclearly encoded RNA-binding proteins (Hammani and Giegé, 2014). Given the relaxed nature of transcription, post-transcriptional processing, such as RNA editing, splicing, maturation of transcript ends and RNA degradation, are known to play predominant roles in shaping the plant mitochondrial transcriptome (Hammani and Giegé, 2014). Mutants of nuclearly encoded mitochondrial RNA processing factors have proven to be useful in probing the physiological roles of mitochondrial gene expression. In particular, studies of C-to-U editing PPR protein genes have led to a collection of about 100 mutants, among which RNA-editing mutants are available for most mitochondrial genes (Takenaka et al., 2019). The majority of the mutations confer visible phenotypes, such as growth retardation, impaired embryo development, late flowering, or reduced pollen sterility (Takenaka et al., 2019). Similar developmental defects are also observed in mutants of genes encoding other mitochondrial proteins, including *ndufs4* (complex I mutant), *rpoTmp* (RNA polymerase mutant), and *atphb3* (prohibitin mutant) (Van Aken et al., 2010). These results suggest that mitochondria play supportive roles in plant growth, presumably by supplying energy through oxidative phosphorylation. However, it is still unclear whether mitochondrial gene expression has a role in the regulation of plant organogenesis (Hammani and Giegé, 2014).

The study of temperature-dependent fasciation (TDF) mutants of Arabidopsis

root redifferentiation defective 1 (rrd1), *rrd2*, and *root initiation defective 4 (rid4)* are temperature-sensitive mutants of Arabidopsis that were originally isolated in our laboratory via screening using adventitious root (AR) formation from hypocotyl tissue segments as an index phenotype (Konishi and Sugiyama, 2003; Sugiyama, 2003). In addition to AR formation, other aspects of development, such as seedling growth (Fig. 2A) and callus

formation, were affected by high-temperature conditions (Konishi and Sugiyama, 2003; Sugiyama, 2003). Most notable among these aspects was their LR phenotype, in which abnormally broadened (i.e., fasciated) LRs were formed at 28°C (non-permissive temperature), but not at 22°C (permissive temperature), in a tissue culture setting (Fig. 2B); thus, we termed the three mutants as temperature-dependent fasciation (TDF) mutants (Otsuka and Sugiyama, 2012). It was also revealed that the early stages of LR development are affected in the TDF mutants (Fig. 3), and that the fasciated LRs exhibit exclusive enlargement of inner tissues (Otsuka and Sugiyama, 2012), suggesting that the genes responsible for the TDF mutations (TDF genes) encode negative regulators of proliferation that are important for the size restriction of the central zone during the formation of early stage LR primordia.

Surprisingly, positional cloning later revealed that all TDF genes encode RNA processing factors that show mitochondrial localization (Otsuka, 2012; Otsuka et al., 2020). *RRD1* encoded a poly(A)-specific ribonuclease (PARN)-like protein (Fig. 4). PARN belongs to the DEDD superfamily of deadenylases (Pavlopoulou et al., 2013), and shows a strong preference for adenine as a substrate (Lee et al., 2019; Pavlopoulou et al., 2013; Virtanen et al., 2013). Since its discovery in animal cells (Körner and Wahle, 1997; Körner et al., 1998), the primary role of PARN has been assumed to be the regulation of mRNA metabolism. However, accumulating evidence suggests that the targets of PARN may be limited to certain subsets of mRNAs and/or biological contexts (Lee et al., 2019). Recent human and animal studies have led to an increased appreciation of its participation in the maturation process of a wide variety of noncoding RNAs (Lee et al., 2019). In plants, PARN was found to play a distinct role in the removal of the poly(A) tails of mitochondrial mRNA (Hirayama, 2014; Hirayama et al., 2013; Kanazawa et al., 2020). The sequence similarity of *RRD1* to PARN (Reverdatto et al., 2004) and its mitochondrial localization, therefore points to the possibility that *RRD1* may also be involved in regulating the poly(A) status of mitochondrial mRNA; however experimental evidence remains inconclusive (Otsuka, 2012).

RRD2 and *RID4* both encoded a pentatricopeptide repeat (PPR) protein (Fig. 4). The PPR protein family has undergone a remarkable expansion in land plants, representing one of the largest protein families thereof (Barkan and Small, 2014). PPR proteins are known for their role in regulating various aspects of organellar post-transcriptional gene expression, such as RNA stabilization, RNA cleavage, RNA splicing, RNA editing, and translation

(Barkan and Small, 2014; Hammani and Giegé, 2014). They are characterized by the tandem assembly of degenerate protein motifs of about 35 amino acids, termed PPR motifs (Barkan and Small, 2014). The PPR motifs allow PPR proteins to recognize specific sites of single-stranded RNAs through a one-motif to one-base interaction (Barkan and Small, 2014). The mitochondrial localization of RRD2 and RID4, shown in previous studies (Otsuka, 2012; Otsuka et al., 2020) indicated their involvement in mitochondrial RNA processing, however their molecular function remains unclear.

Purpose of thesis

The main purpose of this thesis is to uncover the mechanisms that control cell proliferation during early stages of LR organogenesis in Arabidopsis. Although Arabidopsis LR development has been established as an excellent model to investigate the molecular underpinnings of plant organogenesis, little is still known about the factors required for the local fine-tuning of cell proliferation which takes place after organ initiation. Previous work in our lab have identified three temperature-dependent fasciation (TDF) mutants of Arabidopsis, *root redifferentiation defective 1 (rrd1)*, *rrd2*, and *root initiation defective 4 (rid4)*, which are characterized by the formation of abnormally broadened (i.e., fasciated) LRs under high-temperature conditions due to excessive cell division. The TDF genes, *RRD1*, *RRD2*, and *RID4* all encode putative RNA processing factors that reside in mitochondria. The further study of the TDF mutants would lead to our better understanding of the mechanisms by which plants restrict cell division in order to form of properly sized and structured organs. It would also be a pioneering study on the previously undiscovered link between organellar RNA processing and plant organ morphogenesis.

This thesis first focuses on the molecular functions of each TDF gene. I describe the involvement of RRD1 in degradation of poly(A) tails of mitochondrial mRNA, as well as the participation of RRD2 and RID4 in mitochondrial mRNA editing. I further reveal that all TDF mutants carry defects in the biosynthesis of the electron transport chain components. *rrd1* and *rrd2* show decreased cytochrome *c* levels at high temperature, whereas *rid4* shows a dramatic reduction in complex V (ATP synthase) levels regardless of temperature conditions. The observed influence of *rrd1* on cytochrome *c* levels also leads to the discovery of a relationship between the poly(A) status and RNA editing levels in *cytochrome c biogenesis factor 3 (ccb3)* mRNA. By performing pharmacological analysis, I also show that the generation of reactive oxygen species (ROS) might be a trigger of excessive cell division

in the TDF mutants. Finally, I discuss possible mechanisms of ROS-induced LR fasciation. Altogether, this study aims to provide novel insights into the molecular machinery involved in mitochondrial RNA processing and their relationship to cell division control during plant organogenesis.

Chapter 2. Results

Analysis of the role of RRD1 in poly(A) degradation of mitochondrial mRNAs

PARN belongs to the DEDD superfamily of deadenylases (Pavlopoulou et al., 2013). Recent human and animal studies have led to an increased appreciation of its participation in the maturation process of a wide variety of noncoding RNAs (Lee et al., 2019). In plants, however, PARN plays a distinct role in the removal of the poly(A) tails of mitochondrial mRNA (Hirayama, 2014; Hirayama et al., 2013; Kanazawa et al., 2020). The sequence similarity to PARN (Reverdatto et al., 2004) and its mitochondrial localization, points to the possibility that RRD1 may also be involved in regulating the poly(A) status of mitochondrial mRNA. Previously, a microarray analysis of poly(A)⁺ RNAs prepared from wild-type and *rrd1* explants induced to form LR at 28°C had been performed (Otsuka, 2012). A substantial increase in the levels of a few mitochondria-encoded poly(A)⁺ transcripts in *rrd1* explants was shown in this study. Therefore, I reanalyzed the microarray data and found that the overwhelming majority of genes which showed elevated signals in *rrd1* were mitochondrial genes (Fig. 5A). All transcripts of functionally characterized mitochondrial genes, with the exception of *nad5C*, showed increased abundance in *rrd1* (Fig. 5B and C, Table 2). As the majority of plant mitochondrial transcripts normally lack poly(A) tails, presumably because of swift removal after its addition (Holec et al., 2008), it was suspected that the apparent sharp increase in poly(A)⁺ mitochondrial transcript level might be ascribed to defective poly(A) tail removal, rather than increased transcription. In fact, a comparative analysis of polyadenylated and total RNA levels via quantitative reverse transcription polymerase chain reaction (qRT-PCR) revealed a selective increase in polyadenylated transcripts (Fig. 6). Furthermore, a circularized RNA (CR)-RT PCR analysis (Forner et al., 2007) of the *cytochrome oxidase subunit 1 (cox1)* mRNA was performed to study its 3' extremity, and revealed a marked increase in the polyadenylated to non-polyadenylated ratio in *rrd1* compared with the wild-type plant (Fig. 7). In addition, a poly(A) test assay by rapid amplification of cDNA ends (RACE-PAT) (Sallés et al., 1999) showed that polyadenylated transcript levels were increased at higher temperature in *rrd1* (Fig. 8). Taken together, these results demonstrated that RRD1 is involved in poly(A) tail removal in mitochondrial mRNAs, and that, in *rrd1*, polyadenylated mitochondrial transcripts accumulate in a temperature-dependent manner.

To assess the effects of the observed accumulation of poly(A)⁺ mitochondrial transcripts in *rrd1*, I introduced the *ahg2-1* suppressor 1 (*ags1*) mutation into *rrd1*. *ags1* is a mutation of a mitochondrion-localized poly(A) polymerase (PAP), AGS1, which was originally identified based on its ability to counteract AtPARN/AHG2 loss of function (Hirayama et al., 2013). A substantial decrease in mitochondrial poly(A)⁺ transcript levels was observed in the *rrd1 ags1* double mutant compared with the *rrd1 AGS1* control (Fig. 9A). Moreover, *rrd1* phenotypes, such as temperature-dependent seedling growth retardation (Fig. 9B) and LR fasciation, were significantly alleviated (Fig. 10). These results indicate that the accumulation of poly(A)⁺ mitochondrial transcripts is the primary cause of the *rrd1* phenotype.

Analysis of the roles of RRD2 and RID4 in mitochondrial mRNA editing

PPR proteins are known for their role in regulating various aspects of organellar post-transcriptional gene expression, such as RNA stabilization, RNA cleavage, RNA splicing, RNA editing, and translation (Barkan and Small, 2014; Hammani and Giegé, 2014). They are characterized by the tandem assembly of degenerate protein motifs of about 35 amino acids, termed PPR motifs (Barkan and Small, 2014). The PPR motifs allow PPR proteins to recognize specific sites of single-stranded RNAs through a one-motif to one-base interaction (Barkan and Small, 2014). The PPR protein family has undergone a remarkable expansion in land plants, representing one of the largest protein families thereof (Barkan and Small, 2014). RRD2 and RID4 belong to the PLS-class of PPR proteins, most of which have been reported as being C-to-U RNA editing factors (Kobayashi et al., 2019). The PLS class PPR proteins contain three types of PPR motifs, the P motif (normally 35 a. a. in length), the L motif (35–36 a. a. (long)) and the S motif (31 a. a. (short)), in contrast to the P-class PPR proteins, which only contain P motifs (Barkan and Small, 2014; Cheng et al., 2016). Considering their localization to mitochondria (Otsuka, 2012; Otsuka et al., 2020), I speculated on the involvement of RRD2 and RID4 in the editing of mitochondrial RNA. A comprehensive sequence analysis of previously reported RNA editing sites using cDNA prepared from explants induced to form LR s at 28°C revealed an almost complete abolishment of C-to-U editing at two sites (*cytochrome c biogenesis protein 2 (ccb2)*-71C and *ccb3*-575C) in *rrd2* and at six sites (*ATP synthase subunit 4 (atp4)*-395C, *ribosomal protein l5 (rpl5)*-58C, *rpl5*-59C, *rps3*-1344C, *rps4*-77C, and *rps4*-332C) in *rid4* (Fig. 11 and 12A). Editing was also completely abolished in these sites at 22°C (Fig. 12B). RID4 editing sites showed incomplete editing in *rid4-2*, implying a partial loss of function in this mutant (Fig. 11). Significant

identity was found among the 5' upstream sequences of the editing sites that were affected in each mutant (Fig. 13), further suggesting that RRD2 and RID4 participate in the editing of these sites via direct contact. During the course of my study of RNA editing, the *RRD2* gene (At1g32415) was reported as the gene responsible for the *cell wall maintainer 2 (cwm2)* mutation (Hu et al., 2016); thus, I will refer to it as *RRD2/CWM2* henceforth. The identification of *ccb3-575C* as an RRD2/CWM2 editing site was in agreement with the study of *cwm2* (Hu et al., 2016), whereas *ccb2-71C* was a newly discovered target of RRD2/CWM2.

In addition, all editing sites of *ccb3*, with the exception of those that were unedited in the wild type, showed declining levels of RNA editing in both *rrd2* and *rid4* (Fig. 11). However, these sites were not considered as targets of RRD2 and RID4 for the following reasons. These sites were incompletely edited, even in the wild type, as opposed to most other sites (Fig. 11), suggesting that their editing is relatively slow and highly susceptible to fluctuations in the kinetic balance between editing and transcription. Moreover, editing at these sites was almost unaffected at 22°C (Fig. 16C) and was only partially inhibited at 28°C in *rrd2* and *rid4* (Fig. 11), even though these mutants are assumed to have lost the function of the corresponding genes completely. *ccb3-624C* was also not regarded as a target site, despite the complete absence of editing in both *rrd2* and *rid4*, as it was more likely due to originally low levels of editing compared with other sites in *ccb3* (Fig. 11). This view was reinforced by the lack of similarity in the upstream sequence between *ccb3-624C* and the other editing sites that were strongly affected by the *rrd2* and *rid4* mutations (Fig. 13).

Next, to investigate the effects of losses of function of RRD2/CWM2 and RID4 on mitochondrial protein composition, I performed a blue-native (BN)-PAGE analysis of mitochondrial extracts prepared from seed-derived callus (Fig. 14B) cultured for 3 days at 22°C or 28°C after a 20-day 22°C incubation period. This revealed a substantial loss of complex V (ATP synthase complex) in *rid4* at both 22°C and 28°C culture conditions (Fig. 14A), likely caused by defective mRNA editing of *atp4* (Fig. 14C), which is a component of this protein complex. No noticeable differences were found in *rrd1* and *rrd2*. Because *ccb2* and *ccb3*, the two mitochondrial genes that are targeted by RRD2/CWM2, are related to cytochrome *c* (cyt *c*) maturation (Fig. 15A), I quantified cyt *c* levels in *rrd2*. Cyt *c* levels on a per mitochondrial protein basis were decreased in *rrd2* callus cultured at 28°C for 3 days (Fig. 15, B and C) in two out of three cultures, although the difference was not significant when all three results were included. This decrease in cyt *c* levels in *rrd2* was in accordance

with a previous analysis of *cwm2* (Hu et al., 2016). At 22°C, however, no significant difference was observed between *rrd2* and the wild type. Furthermore, we found that the difference in cyt c levels was more pronounced after longer periods of culture at 28°C (Fig. 15, D and E). These results indicate that, in *rrd2*, cyt c maturation activity was affected to a greater extent at higher temperatures, at least in callus, which possesses root-tissue-like properties (Sugimoto et al., 2010), possibly explaining the temperature-dependent nature of its phenotype. The data reported above demonstrated that, in both *rrd2* and *rid4*, the production of certain components of the mitochondrial electron transport chain is hampered by defective mRNA editing.

Analysis of the relationship between poly(A) status and editing in *ccb3* mRNA

本セクションについては5年以内に雑誌等で刊行予定のため、非公開。

Expression analysis of the TDF genes

Previously, GFP reporters were used to examine the expression patterns of the TDF genes (Otsuka, 2012), in which genomic constructs of *RRD1* and *RID4* encompassing the promoter region to the end of the protein-coding sequence (*RRD1::RRD1:GFP* and *RID4::RID4:GFP*) were introduced into *rrd1* and *rid4-1*, respectively. It was shown that in the root system, GFP expression was mostly confined to the root apical meristem and LR primordia and that during early LR development, GFP expression was particularly strongly expressed in the central region of the primordia. This implied that the expression of TDF genes *RRD1* and *RID4* were largely limited to cells in a mitotically active state.

However, my analysis of mitochondrial RNA editing demonstrated that in the LR-induced root explants of *rid4*, editing of the sites targeted by *RID4* were totally lost, whereas they were completely edited in the WT (Fig. 12). This result suggests that *RID4* participates in RNA editing in non-dividing cells in addition to dividing cells, since the explants used in the study contains fully differentiated and mitotically dormant cells in the endodermis, cortex and epidermis layers. Therefore, I reexamined the expression of *RRD1* and *RID4* in the root (Fig. 19). For both *RRD1::RRD1:GFP* and *RID4::RID4:GFP*, although the signal appeared the strongest in the central region of the LR primordium, GFP expression was also observed in the peripheral regions of the primordium as well as non-LR primordium cells in the stele tissue. In addition, faint GFP signals were observed in the cortex/epidermis tissues. The overall expression pattern, in which strong expression is observed in LR primordia and the stele, while weaker signals are observed in the cortex/epidermis tissues, resembled that of the *35S::Mt-GFP* line, which expresses mitochondria-targeted GFP under the constitutive active cauliflower mosaic virus (CaMV) 35S promoter (Fig. 19). These results suggested that TDF gene action is not exclusive to the central region of LR primordia and that the expression pattern of the TDF genes most likely reflected the abundance of mitochondria.

Effects of defective mitochondrial respiration on LR formation

The results obtained for *rrd1*, *rrd2*, and *rid4* indicate a possible relationship between mitochondrial electron transport and cell division control during LR morphogenesis. In fact, in a previous study (Otsuka, 2012), it was shown that the induction of LRs at 22°C from wild-type explants in the presence of rotenone (complex I inhibitor), antimycin A (complex III inhibitor), or oligomycin (complex V inhibitor) leads to LR fasciation, providing evidence that electron transport chain defects are the cause of the TDF LR phenotype. Capitalizing on

this result, I first tested the effects of antimycin A at different temperatures and found that LR fasciation induced by the drug was more enhanced at higher temperatures (Fig. 20, A–C). It was also found that at lower temperatures, the effect of the treatment was significantly lessened (Fig. 20C). Therefore, I reexamined the effects of the three respiratory inhibitors at 28°C and confirmed that they gave rise to a significant increase in LR width. To further investigate the underlying molecular pathway, I next asked whether either reduced ATP synthesis, or ROS generation, phenomena that are commonly associated with defective mitochondrial respiration might be involved. I found that the respiratory uncoupler carbonylcyanide m-chlorophenyl-hydrazone (CCCP) did not increase LR width (Fig. 21A), although LR growth inhibition was observed in a dose-dependent manner (Fig. 21B), whereas the ROS inducer paraquat (PQ) triggered a significant fasciation of LRs (Fig. 22). Furthermore, the application of the ROS scavenger ascorbate resulted in a reversal of the LR broadening induced by PQ treatment (Fig. 22). The same effect was observed against the *rid4-2* mutation. These data suggest that the increase in the levels of ROS, but not the decrease in the levels of ATP, acts downstream of defective mitochondrial respiration to promote excessive cell division during LR development in the TDF mutants.

Local gradient formation of auxin is important for LR initiation and the subsequent organization of the LR primordium (Benková et al., 2003; Geldner et al., 2004; Lavenus et al., 2013). Strong genetic perturbations of polar auxin transport result in homogeneous proliferation of the pericycle cell layer in large regions of the root upon exogenous auxin treatment. In addition, chemical inhibition of auxin polar transport by naphthylphthalamic acid (NPA) gave rise to broadened LR primordia reminiscent of fasciated LRs of the TDF mutants (Fig. 23). These data indicate a role for local auxin gradient formation in restricting proliferative capacity during LR formation. Therefore, I tested whether ROS-induced LR fasciation is mediated by altered auxin patterning in early LR primordia. The examination of the expression pattern of the auxin-responsive β -glucuronidase marker *DR5::GUS* (Benková et al., 2003; Geldner et al., 2004; De Smet et al., 2010) at early stages of LR induction, however, did not reveal differences between the control and PQ-treated root segments, whereas treatment with NPA resulted in enhanced expression along the entire root segment (Fig. 24). This result indicates that ROS-induced LR fasciation is not caused by an impairment in auxin gradient formation.

Live imaging analysis of LR fasciation using light-sheet microscopy

本セクションについては5年以内に雑誌等で刊行予定のため、非公開。

Chapter 3. Discussion

RRD1 functions in poly(A) tail removal in mitochondrial mRNA

PARN is a 3' exoribonuclease of the DEDD superfamily (Pavlopoulou et al., 2013), which shows a strong preference for adenine (Lee et al., 2019; Pavlopoulou et al., 2013). In plants, PARN is involved in the removal of poly(A) tails from mitochondrial transcripts (Hirayama, 2014; Hirayama et al., 2013; Kanazawa et al., 2020). Here, I studied the functions of *RRD1*, a gene encoding a PARN-like protein (Fig. 4) that resides in mitochondria. Analysis of mitochondrial mRNA in *rrd1* demonstrated the participation of RRD1 in poly(A) tail degradation of mitochondrial mRNA (Fig. 5–10). In plant mitochondria, immature 3' extremities of mRNA, together with irregular RNAs, such as 3' misprocessed mRNAs, rRNA maturation by-products, and cryptic transcripts, are known to be polyadenylated before they are degraded by mitochondrial polynucleotide phosphorylase (mtPNPase) (Holec et al., 2008). In fact, down-regulation of mtPNPase in Arabidopsis results in the accumulation of long preprocessed mRNAs, as well as irregular RNAs, the majority of which are polyadenylated (Holec et al., 2008). In *rrd1*, unusually long preprocessed mRNAs do not seem to accumulate, as the size of RACE-PAT assay products (Fig. 8) corresponded to that of previously reported mature transcript 3' ends. Total mitochondrial mRNA levels were unelevated in *rrd1* (Fig. 6), suggesting that RRD1 is not involved in controlling mRNA abundance by promoting their degradation. Whether by-product accumulation takes place in *rrd1* is not clear. However, given its absence in *ahg2* (Hirayama et al., 2013), this is unlikely. Based on these considerations, I conclude that RRD1 plays a distinct role from mtPNPase and seems to be specifically involved in 3' processing of near-matured mRNA.

Failure in the removal of poly(A) tails from mitochondrial transcripts seems to be the primary cause of the *rrd1* phenotype. This is evidenced by the alleviation of the *rrd1* phenotype by the introduction of a mutation of the mitochondria-localized poly(A) polymerase gene *AGS1* (Fig. 9 and 10). As most protein-coding genes in the Arabidopsis mitochondrial genome are involved in the biogenesis of the electron transport chain (Hammani and Giegé, 2014), it is likely that mitochondria of *rrd1* carry defects in respiratory activity. Unlike the AtPARN/AHG2 loss-of-function mutant *ahg2*, which shows a reduction in complex III levels (Hirayama et al., 2013), no apparent difference in the amount of complex III has been detected in *rrd1* to date (Fig. 14).

本セクションについては5年以内に雑誌等で刊行予定のため、非公開。

RRD2 and RID4 function in mitochondrial mRNA editing

In this study, I examined the molecular functions of *RRD2* and *RID4*, both of which encode a mitochondria-localized PLS-class PPR protein (Fig. 4). *At1g32415* was reported as the gene responsible for the *cwm2* mutant (Hu et al., 2016) during the course of this study. A predominant role for PLS-class PPR proteins in RNA editing has been demonstrated with more than 50 out of a total of approximately 200 of these proteins in *Arabidopsis* having been identified as C-to-U editing factors of mitochondria or plastid RNA (Kobayashi et al., 2019). A comprehensive analysis of mitochondrial RNA editing revealed the abolishment of editing at specific sites in *rrd2* and *rid4* (Fig. 11 and 12). I conclude that both *RRD2/CWM2* and *RID4* are PLS-class PPR proteins that are involved in mitochondrial mRNA editing.

In *rrd2*, editing at 71C of *ccb2* and 575C of *ccb3* was absent (Fig. 12). Both *ccb2* (also known as *ccb206*, *ccmB*, *ABCI2*, and *AtMg00110*) and *ccb3* (also known as *ccb256*, *ccmC*, *ABCI3*, and *AtMg00900*) encode a multisubunit ATP-binding cassette (ABC) protein, which are involved in the maturation of mono hemic *c*-type cytochromes, the soluble cyt *c*, and the membrane-bound cyt *c*₁ of complex III (Giegé et al., 2008; Shevket et al., 2019). Of the two editing sites, *ccb3*-575C was previously reported as a target of *RRD2/CWM2* (Hu et al., 2016), whereas *ccb2*-71C is a newly discovered target. A decrease in the level of cyt *c* was detected in *rrd2*, which is consistent with that reported previously for *cwm2* (Hu et al., 2016). The data demonstrated the role of *RRD2/CWM2* in cyt *c* maturation via the RNA editing of cyt *c* biogenesis factors.

In *rid4*, I observed striking reductions in RNA editing at *atp4*-395C, *rpl5*-58, *rpl5*-59C, *rps3*-1344C, *rps4*-77C, and *rps4*-332C (Fig. 11 and 12). *atp4* (also known as *orf25*, *AtMg00640*) encodes the peripheral stalk protein (subunit b) of the mitochondrial ATP synthase complex (complex V) (Heazlewood et al., 2003). *rpl5*, *rps3*, and *rps4* encode mitochondrial ribosome proteins. Analysis of mitochondrial protein complexes showed a dramatic decrease in the level of complex V in *rid4*, probably because of impaired editing of *atp4*-395C. This is similar to the *organelle transcript processing 87* (*otp87*) mutant of

Arabidopsis, in which editing of *atp1*-1178C is deficient (Takenaka et al., 2019). These data showed that the formation of complex V could be disrupted by defective RNA editing at a single site of a subunit gene. Considering that the C-to-U editing of the *rps4* transcript at a different site (*rps4*-377) has been shown to affect mitochondrial ribosome assembly in the *growing slowly 1* (*grs1*) mutant (Takenaka et al., 2019), it is possible that the *rid4* mutation also has an impact on the mitochondrial ribosome.

Recent advances in the mechanistic understanding of RNA binding by PLS-class PPR proteins have led to the identification of residues at certain positions within the PPR motifs that are important for ribonucleotide recognition (Barkan and Small, 2014; Kobayashi et al., 2019). By mapping these residues of previously reported RNA-editing PPR proteins to their binding sites, which are located 5' upstream of the editing sites, the so-called 'PPR code' has been elucidated, thus enabling the matching of PPR proteins to their candidate editing targets, and vice versa (Kobayashi et al., 2019). According to the recently refined PPR code prediction (Kobayashi et al., 2019), RID4 was highly ranked as a potential binding protein of *atp4*-395C (18th, $P = 4.35 \times 10^{-2}$), *rpl5*-58C (5th, $P = 3.04 \times 10^{-2}$) and *rps4*-332C (2nd, $P = 4.06 \times 10^{-3}$). Conversely, these sites were among the predicted editing sites of RID4 ($P < 0.05$) (Kobayashi et al., 2019). With regard to RRD2, however, the newly identified binding site (*ccb2*-71C) ranked very low, despite the incorporation of RRD2/CWM2 binding to *ccb3*-575C as learning data for the PPR code prediction (Kobayashi et al., 2019). This discrepancy may be related to the unusual arrangement of PPR motifs in RRD2/CWM2, in which repeats of SS motifs are prevalent, in contrast to canonical PLS-class PPRs, which follow the (P1-L1-S1)_n-P2-L2-S2 pattern, such as RID4 (Fig. 4) (Cheng et al., 2016). Nevertheless, given the similarity between the upstream sequences of editing sites which are severely affected by *rrd2* and *rid4* (Fig. 13), they are likely edited by RRD2/CWM2 and RID4 via direct interaction. The presented data will contribute to the improvement of PPR protein target estimation.

Editing of mitochondrial mRNA is influenced by its poly(A) status

本セクションについては5年以内に雑誌等で刊行予定のため、非公開。

The origins of the temperature sensitivity may differ among the TDF mutants

A distinct feature of the TDF phenotype is its exclusive observation at high-temperature conditions (Konishi and Sugiyama, 2003; Otsuka and Sugiyama, 2012; Sugiyama, 2003). My study revealed some differences in the origin of temperature sensitivity among the TDF mutants. The *rrd1* mutation causes a truncation of the C-terminal domain of the RRD1 protein (Fig. 4). This finding, together with the enhancement of poly(A)⁺ mitochondrial mRNA accumulation at elevated temperatures (Fig. 8), implies that, in *rrd1*, RRD1 is partially functional at least at the permissive temperature, and that its activity is more severely affected at the non-permissive temperature. In contrast, the *rrd2* and *rid4-1* mutations introduce a stop codon close to the N-terminus of RRD2/CWM2 and RID4, respectively, likely resulting in the total loss of their functions (Fig. 4). The complete abolishment of RNA editing of the RRD2 and RID4 target sites in the *rrd2* and *rid4-1* mutants, regardless of temperature (Fig. 12), further supported this idea. However, in *rrd2*, deficient cyt c biogenesis was observed only at high temperature (Fig. 15). This might be accounted for by the temperature sensitivity of the function of either *ccb2* or *ccb3*, which exhibit alteration of the amino acid sequence in *rrd2*, because of impaired RNA editing (Fig. 12). In *rid4-1*, a huge reduction in complex V biosynthesis was observed both at permissive and non-permissive temperatures (Fig. 14). These results suggest that complex V deficiency is more deleterious at higher temperatures, which can explain the temperature sensitivity of the LR fasciation phenotype of *rid4-1*.

Impaired mitochondrial electron transport causes LR fasciation likely via ROS production

The phenocopy of the LR fasciation phenotype of the TDF mutants by treatment with respiratory inhibitors demonstrated the causal relationship between defective mitochondrial electron transport and excessive cell division during early LR development (Fig. 20). Mitochondrial electron transport is best known for its role in driving ATP synthesis through oxidative phosphorylation. Given the lack of LR fasciation after treatment with the mitochondrial uncoupler CCCP (Fig. 21), reduced ATP production seems unlikely to be the cause of LR fasciation. The fact that the huge reduction in complex V levels observed in *rid4* (Fig. 14) does not lead to LR fasciation at the permissive temperature (Otsuka and Sugiyama, 2012) is also supportive of this idea. Experiments using the ROS inducer PQ and the antioxidant ascorbate (Fig. 22) pointed to mitochondrial ROS generation as the potential

trigger of LR fasciation. A previous study also observed enhanced cell division after the application of another ROS inducer, alloxan, during auxin-induced LR formation (Pasternak et al., 2005). In agreement with this ‘ROS hypothesis’, all three respiratory inhibitors used in this study (rotenone, antimycin A, and oligomycin) are potent inducers of oxidative stress (Willems et al., 2016).

ROS-induced LR fasciation is not attributable to a failure in auxin-gradient formation

ROS have been implicated in stress-induced morphogenic responses (SIMR) (Potters et al., 2009). Several studies have shown the involvement of phytohormonal regulation in ROS-triggered SIMR. Altered auxin levels and/or distribution have been proposed as potential mediators in the modulation of cell proliferation in response to oxidative stress (Pasternak et al., 2005; Potters et al., 2009). Several recent studies have found antagonistic interactions between auxin signaling and mitochondrial ROS (Huang et al., 2016). Auxin is a critical factor in LR development, and the centripetal auxin-gradient formation in early-stage LR primordia is thought to contribute to the organization of the LR primordium (Benková et al., 2003; Geldner et al., 2004). However, neither the pattern nor the intensity of the auxin response visualized by the *DR5::GUS* reporter seemed to be altered under PQ treatment, in contrast to the diffuse pattern observed after the application the auxin polar transport inhibitor NPA (Fig. 24). This indicates that ROS-induced LR fasciation is not attributable to a failure in auxin-gradient formation. Further studies of LR fasciation caused by oxidative stress will elucidate novel aspects of the control of cell proliferation during plant organogenesis.

Mitochondrial RNA processing is linked to the control of cell proliferation

Mutants of nuclearly encoded mitochondrial RNA processing factors have proven to be useful in probing the physiological roles of mitochondrial gene expression. In particular, studies of C-to-U editing PPR protein genes have led to a collection of about 100 mutants, among which RNA-editing mutants are available for most mitochondrial genes (Takenaka et al., 2019). The majority of the mutations confer visible phenotypes, such as growth retardation, impaired embryo development, late flowering, or reduced pollen sterility (Takenaka et al., 2019). Similar developmental defects are also observed in mutants of genes encoding other mitochondrial proteins, including *ndufs4* (complex I mutant), *rpoTnp* (RNA polymerase mutant), and *atphb3* (prohibitin mutant) (Van Aken et al., 2010). These results suggest that mitochondria play a supportive role in plant growth, presumably by supplying

energy through oxidative phosphorylation. In this study, however, I demonstrated that RRD1, RRD2, and RID4, genes required for preventing excessive cell division during LR primordium formation, function in mitochondrial RNA processing. This suggests that mitochondrial gene expression not only supports active cell proliferation for growth and development but also participates in the local fine-tuning of organ morphogenesis by restricting cell proliferation. Hence, this study provides a novel clue for the physiological significance of mitochondrial activities in the restrictive regulation of cell proliferation required for the proper morphogenesis of plant organs.

In this study, I first examined the molecular functions of each TDF gene and revealed the involvement of RRD1 in degradation of poly(A) tails of mitochondrial mRNA, as well as the participation of RRD2 and RID4 in mitochondrial mRNA editing. I further found that all TDF mutants carry defects in the biosynthesis of the electron transport chain components. *rrd1* and *rrd2* show decreased cytochrome *c* levels at high temperature, whereas *rid4* shows a dramatic reduction in complex V (ATP synthase) levels regardless of temperature conditions. Pharmacological analysis using mitochondrial respiratory inhibitors, a ROS inducer and a ROS scavenger suggested that the generation of ROS resulting from defective mitochondrial respiration might be the trigger of excessive cell division in the TDF mutants. Although further analysis is necessary, live imaging data hinted that the disruption in the coordination of the patterns of cell division within the primordium might be the cause of ROS-induced LR fasciation. Since examination of auxin response indicated that altered ROS-induced LR fasciation is not attributable to a failure in auxin-gradient formation, future studies on the molecular pathway of ROS-induced LR fasciation is expected to reveal a novel mechanism of cell proliferation control during LR organogenesis, which does not involve the regulation of centripetal auxin accumulation.

本セクションについては5年以内に雑誌等で刊行予定のため、非公開。

Chapter 4. Materials and Methods

Plant materials and growth condition

Arabidopsis thaliana (L.) Heynh. ecotypes Columbia (Col) and Landsberg *erecta* (*Ler*) were used as *Arabidopsis* in this work. The TDF mutants *rrd1*, *rrd2*, and *rid4-1* were described previously (Konishi and Sugiyama, 2003; Otsuka and Sugiyama, 2012; Sugiyama, 2003). The *ags1* mutant (*ags1-1*) was also described previously (Hirayama et al., 2013). The *35S::Mt-GFP* line was a gift from Shin-ichi Arimura (Arimura and Tsutsumi, 2002). *rid4-2* was derived from an ethyl methanesulfonate-mutagenized population of the *Ler* strain of *Arabidopsis*. *rrd1* mutant strains harboring either *ags1* or *AGSI^c* were obtained by *rrd1* (*Ler* background) × *ags1* (Col background) and *rrd1* × Col crosses, respectively. *rrd2* mutant strains harboring either *ags1* or *AGSI^c* were obtained by the same method. The *DR5::GUS* line (Ulmasov et al., 1997) was a gift from Tom J. Guilfoyle and was crossed three times to *Ler* before use. Primers for the genotyping the mutants are listed in Table 1.

For tissue culture experiments, donor plants were aseptically grown on Murashige–Skoog medium supplemented with 1.0% (w/v) sucrose, buffered to pH 5.7 with 0.05% (w/v) 2-morpholinoethanesulfonic acid (MES), and solidified with 1.5% (w/v) agar under continuous light (10–15 $\mu\text{mol m}^{-2} \text{s}^{-1}$) at 22°C. For observation of seedling phenotypes, plants were aseptically grown on the same medium solidified with 1.5% (w/v) agar or 0.8% (w/v) gellan gum under continuous light (50–80 $\mu\text{mol m}^{-2} \text{s}^{-1}$) at 22°C or 28°C. For self-propagation and crossing, plants were grown on vermiculite under continuous light (approximately 50 $\mu\text{mol m}^{-2} \text{s}^{-1}$) at 22°C unless otherwise indicated.

LR induction

As described previously (Ohtani et al., 2010), explants were prepared from 4-day-old seedlings grown on agar plates, and cultured on root-inducing medium (RIM) under continuous light (15–25 $\mu\text{mol m}^{-2} \text{s}^{-1}$) for the induction of semi-synchronous formation of LRs. RIM was B5 medium supplemented with 2.0% (w/v) glucose and 0.5 mg l⁻¹ indole-3-butyric acid, buffered to pH 5.7 with 0.05% (w/v) MES, and solidified with 0.25% (w/v) gellan gum. Culture temperature was set to 22°C for the permissive condition and to 28°C for the non-permissive condition.

Histological analysis

For whole-mount observation, tissue samples were fixed in 25 mM sodium phosphate buffer (pH 7.0) containing 2% (w/v) formaldehyde and 1% (w/v) glutaraldehyde, rinsed with 100 mM sodium phosphate buffer (pH 7.0), and cleared with an 8:1:2 (w/v/v) mixture of chloral hydrate, glycerin, and water. Observations were made with a microscope equipped with Nomarski optics (BX50-DIC; Olympus) to obtain differential interference contrast (DIC) images.

For histochemical detection of GUS reporter expression, tissue samples were fixed in 90% (v/v) acetone overnight at -20°C , rinsed with 100 mM sodium phosphate (pH 7.0), and incubated in X-Gluc solution [0.5 mg ml^{-1} 5-bromo-4-chloro-3-indolyl β -D-glucuronide cyclohexylammonium salt, 0.5 mM potassium ferricyanide, 0.5 mM potassium ferrocyanide, 100 mM sodium phosphate (pH 7.4)] for 140 min at 37°C . After rinsing with 100 mM sodium phosphate buffer (pH 7.0), the samples were mounted on glass slides with an 8:1:2 (w/v/v) mixture of chloral hydrate, glycerin, and water, and then subjected to DIC microscopy.

Expression and localization analysis of GFP reporters

Expression patterns of *RRD1* and *RID4* were examined with transgenic plants harboring *RRD1::RRD1:GFP* and *RID4::RID4:GFP*, respectively. Roots of 6-day-old seedlings of these plants were counterstained with 10 mg l^{-1} of propidium iodide and fluorescence images were obtained using a confocal microscope (FV3000; Olympus). Expression analysis of *35S::Mt-GFP* was performed in the same conditions using a different confocal microscope (FV1200; Olympus).

Microarray analysis and data processing

Microarray data was obtained in a previous study in our laboratory (Otsuka et al., 2020). Briefly, total RNA was extracted with TRIzol reagent (Invitrogen) from explants that had been cultured on RIM for 12 hours in the semi-synchronous LR induction system and purified using the RNeasy microkit (QIAGEN). Affymetrix ATH1 microarrays were hybridized with biotinylated cRNA targets prepared from the RNA samples according to the manufacturer's instructions. It should be noted here that all the targets were derived from poly(A)⁺ RNA in principal because the T7-oligo(dT)₂₄ primer was used for reverse-transcription at the first step of target preparation. Experiments were performed in biological triplicates.

The data sets obtained were processed with a variant of MAS5.0 utilizing robust radius-minimax estimators (Kohl and Deigner, 2010). Differential gene expression was identified

by RankProd 2.0 (Del Carratore et al., 2017). The details of the microarray data was deposited in the Gene Expression Omnibus (<http://www.ncbi.nlm.nih.gov/geo/>) under accession number GSE34595.

Analysis of mRNA polyadenylation status with RACE-PAT

RACE-PAT was performed principally according to (Sallés et al., 1999). Total RNA was extracted with TRIzol reagent (Invitrogen) either from LR-induced explants or seedlings. Total RNA was treated with RNase-free DNase I (Promega) to eliminate genomic DNA, and reverse-transcribed with T7-oligo(dT)₂₄ as a primer using the PrimeScript II 1st strand cDNA Synthesis kit (TaKaRa). Then the poly(A) tail status was analyzed by PCR with a combination of gene-specific and T7 promoter primers. The thermal cycling program consisted of initial 2-minute denaturation at 95°C followed by 30 cycles of 20 seconds at 95°C, 20 seconds at 57°C, and 10 seconds at 72°C. Primers for the RACE-PAT are listed in Table 1.

qRT-PCR analysis

For qRT-PCR, total RNA was extracted with TRIzol reagent (Invitrogen) from explants LR-induced at 28°C for 12 hours. To eliminate genomic DNA, total RNA was treated with RNase-free DNase I (Promega), and reverse-transcribed with a random hexamer or oligo(dT)₂₄ primer using SYBR Premix ExTaq II (TaKaRa). qRT-PCR reactions were performed with gene-specific forward and reverse primers using the PrimeScript RT-PCR kit (TaKaRa) on the StepOne Real-Time PCR system (Applied Biosystems). The thermal cycling program consisted of initial 30-second denaturation at 95°C followed by 40 cycles of 5 seconds at 95°C and 30 seconds at 60°C. At the end of run, melting curves were established for each PCR product to check the specificity of amplification. Expression levels of mRNAs of interest were normalized relative to *TUBULIN4* (At5g44340) expression. DNA fragments amplified from poly(A)⁺ transcripts of several genes including *cob* were sequenced to check the occurrence of mitochondrial editing, which confirmed that they are derived from the mitochondrial genome but not from their copies present in chromosome 2 (Stupar et al., 2001). Experiments were performed in biological triplicates. Primers for the qRT-PCR analysis are listed in Table 1.

CR-RT PCR analysis of the 3' end of mRNA

CR-RT PCR analysis was performed principally according to (Forner et al., 2007). Total RNA was extracted with TRIzol reagent (Invitrogen) from seedlings that had been cultured for 7 days at 22°C and then 2 days at 28°C. To eliminate genomic DNA, total RNA was treated with DNase I (RT grade; Nippon Gene). Next 1 µg of total RNA was circularized with T4 RNA ligase (Promega), desalted with Amicon Ultra 0.5ml (10K; Merck Millipore), and then reverse-transcribed with a *coxI* specific primer (Atcox1-1; Table 1) using M-MLV (Moloney Murine Leukemia Virus) Reverse Transcriptase (RNase H minus, point mutant; Promega). The RNA template was degraded by adding 1/5 volume of 1 M NaOH to the reaction mixture and incubating at room temperature for 10 minutes. The solution was neutralized by adding 1 M HCl and the cDNA was purified with the illustra GFX PCR DNA and Gel Band Purification Kit (GE Healthcare). The 5'-3' junction sequence was amplified by PCR with *coxI* specific primers Atcox1-5'(-176..-196) and Atcox1-3'(17..+38) using Ex Taq Hot Start Version (Takara). The thermal cycling program consisted of initial 4 minute-denaturation at 95°C, followed by 40 cycles of 20 seconds at 95°C, 20 seconds at 50°C, and 40 seconds at 72°C. The PCR products were purified with the Wizard SV Gel and PCR Clean-Up System (Promega) and cloned into the pGEM-T Easy Vector (Promega) using DNA Ligation Kit <Mighty Mix> (Takara). The constructed vector was transformed into the DH5α strain of *E. coli*, and about 20 clones were sequenced. Primers for the CR RT-PCR analysis are listed in Table 1.

Analysis of mitochondrial mRNA editing

For the analysis of mitochondrial mRNA editing, total RNA was extracted with TRIzol reagent (Invitrogen) from explants LR-induced at 28°C for 12 hours. Total RNA was treated with RNase-free DNase I (Promega), and reverse-transcribed with a random hexamer using the PrimeScript II 1st strand cDNA Synthesis kit (TaKaRa). Gene specific primers were used to amplify cDNA by PCR using Ex Taq Hot Start Version (Takara). The thermal cycling program consisted of initial 4-minute denaturation at 95°C followed by 30 to 40 cycles of 30 seconds at 95°C, 30 seconds at 55°C, and 90 to 120 seconds at 72°C. The PCR products were purified either by ExoStar DNA purification reagent (GE Healthcare) or Wizard SV Gel and PCR Clean-Up System (Promega), and then sequenced.

Analysis of mitochondrial protein

Isolation of intact mitochondria was performed principally according to (Murcha and Whelan, 2015). Seed-derived callus cultured in liquid callus-inducing medium (CIM) (Konishi and

Sugiyama, 2003; Sugiyama, 2003) in the dark with gentle shaking was used as starting material. About 16 g of callus was homogenized in 40 ml ice-cold grinding buffer (0.3 M Mannitol, 50 mM Tetrasodium pyrophosphate, 2 mM EDTA (Disodium salt), 0.5 % (w/v) PVP-40, 0.5 % (w/v) BSA, 20 mM L-cysteine, pH 8.0 (HCl)) with a mortar, pestle, and glass beads (0.4-mm diameter). The homogenate was filtered through four layers of Miracloth (Millipore) and centrifuged at 2,300g for 5 minutes twice. The resulting supernatant was centrifuged at 18,000g for 10 minutes. The resulting pellet was resuspended in wash buffer (0.3 M Mannitol, 10 mM *N*-Tris(hydroxymethyl)methyl-2-aminoethanesulfonic acid (TES), 0.1% (w/v) BSA, pH 7.5 (NaOH)) and layered over a three-step Percoll (GE Healthcare) gradient (40%, 21%, and 16% (v/v)). The gradient was centrifuged at 23,500 rpm (approximately 40,000g to 70,000g) for 30 minutes. Mitochondria were collected from the 21% and 40% interface and washed twice in wash buffer (without BSA) by centrifugation at 18,000g for 10 minutes.

For BN-PAGE analysis, 10 µg protein of mitochondria was solubilized in 12 µL Native PAGE Sample Buffer (1% n-dodecyl-β-D-maltoside (DDM), Thermo Fisher Scientific), mixed with 1.8 µL of sample additive (33.3% (w/v) glycerol, 1.67% (w/v) Coomassie Brilliant Blue (CBB) G250), and then separated by electrophoresis on a NativePAGE 4 to 16%, Bis-Tris Gel (Thermo Fisher Scientific).

For immunoblot analysis, proteins separated via SDS-PAGE were transferred to a PVDF membrane and exposed to a primary antibody against cyt c (AS08 343A, Agrisera; 1:5000 dilution). As a secondary antibody, I used a peroxidase-labeled anti-rabbit antibody (NIF824, GE Healthcare; 1:5000 dilution). Immunodetection was performed by incubating the membranes in the Western BLoT Quant HRP Substrate (Takara) and recording the chemiluminescence by LuminoGraph I (ATTO).

Live-imaging analysis of LR formation

Live-imaging of LR primordium development was performed according to (von Wangenheim et al., 2017) with some modifications using the Lightsheet Z.1 microscope (ZEISS). Root segments from 4-day old *AUX1::AUX1:YFP* seedlings were first cultured on solid RIM (0.6% gellan gum) for approximately 6 hours prior to imaging. The root segments were attached to a solid RIM gel block using 1% low melting agarose (Promega). The block was glued onto a piece of glass that attached to a glass capillary using 1% low melting agarose.

The capillary was loaded onto the microscope for imaging. The observation chamber was perfused with liquid RIM using a peristaltic pump (ATTO).

Chapter 5. References

- Van Aken, O., Whelan, J., and Van Breusegem, F. (2010). Prohibitins: mitochondrial partners in development and stress response. *Trends Plant Sci.* *15*, 275–282.
- Arimura, S., and Tsutsumi, N. (2002). A dynamin-like protein (ADL2b), rather than FtsZ, is involved in *Arabidopsis* mitochondrial division. *Proc. Natl. Acad. Sci. U. S. A.* *99*, 5727–5731.
- Barkan, A., and Small, I. (2014). Pentatricopeptide Repeat Proteins in Plants. *Annu. Rev. Plant Biol.* *65*, 415–442.
- Benitez-Alfonso, Y., Faulkner, C., Pendle, A., Miyashima, S., Helariutta, Y., and Maule, A. (2013). Symplastic intercellular connectivity regulates lateral root patterning. *Dev. Cell* *26*, 136–147.
- Benková, E., Michniewicz, M., Sauer, M., Teichmann, T., Seifertová, D., Jürgens, G., and Friml, J. (2003). Local, efflux-dependent auxin gradients as a common module for plant organ formation. *Cell* *115*, 591–602.
- Berckmans, B., Vassileva, V., Schmid, S.P.C., Maes, S., Parizot, B., Naramoto, S., Magyar, Z., Lessa Alvim Kamei, C., Koncz, C., Bögre, L., Persiau, G., de Jaeger, G., Friml, J., Simon, R., Beeckman, T., and de Veylder, L. (2011). Auxin-Dependent cell cycle reactivation through transcriptional regulation of *Arabidopsis* E2Fa by lateral organ boundary proteins. *Plant Cell* *23*, 3671–3683.
- Del Carratore, F., Jankevics, A., Eisinga, R., Heskes, T., Hong, F., and Breitling, R. (2017). RankProd 2.0: a refactored bioconductor package for detecting differentially expressed features in molecular profiling datasets. *Bioinformatics* *33*, 2774–2775.
- Cheng, S.F., Gutmann, B., Zhong, X., Ye, Y.T., Fisher, M.F., Bai, F.Q., Castleden, I., Song, Y., Song, B., Huang, J.Y., Liu, X., Xu, X., Lim, B.L., Bond, C.S., Yiu, S.M., and Small, I. (2016). Redefining the structural motifs that determine RNA binding and RNA editing by pentatricopeptide repeat proteins in land plants. *Plant J.* *85*, 532–547.

Du, Y.J., and Scheres, B. (2017). PLETHORA transcription factors orchestrate de novo organ patterning during *Arabidopsis* lateral root outgrowth. *Proc. Natl. Acad. Sci. U. S. A.* *114*, 11709–11714.

Fernandez, A., Drozdzecki, A., Hoogewijs, K., Vassileva, V., Madder, A., Beeckman, T., and Hilson, P. (2015). The GLV6/RGF8/CLEL2 peptide regulates early pericycle divisions during lateral root initiation. *J. Exp. Bot.* *66*, 5245–5256.

Förner, J., Weber, B., Thuss, S., Wildum, S., and Binder, S. (2007). Mapping of mitochondrial mRNA termini in *Arabidopsis thaliana*: t-elements contribute to 5' and 3' end formation. *Nucleic Acids Res.* *35*, 3676–3692.

Geldner, N., Richter, S., Vieten, A., Marquardt, S., Torres-Ruiz, R.A., Mayer, U., and Jürgens, G. (2004). Partial loss-of-function alleles reveal a role for GNOM in auxin transport-related, post-embryonic development of *Arabidopsis*. *Development* *131*, 389–400.

Giegé, P., and Brennicke, A. (1999). RNA editing in *Arabidopsis* mitochondria effects 441 C to U changes in ORFs. *Proc. Natl. Acad. Sci.* *96*, 15324–15329.

Giegé, P., Hoffmann, M., Binder, S., and Brennicke, A. (2000). RNA degradation buffers asymmetries of transcription in *Arabidopsis* mitochondria. *EMBO Rep.* *1*, 164–170.

Giegé, P., Grienenberger, J.M., and Bonnard, G. (2008). Cytochrome *c* biogenesis in mitochondria. *Mitochondrion* *8*, 61–73.

Goh, T. (2019). Long-term live-cell imaging approaches to study lateral root formation in *Arabidopsis thaliana*. *Microscopy* *68*, 4–12.

Goh, T., Joi, S., Mimura, T., and Fukaki, H. (2012). The establishment of asymmetry in *Arabidopsis* lateral root founder cells is regulated by LBD16/ASL18 and related LBD/ASL proteins. *Development* *139*, 883–893.

Goh, T., Toyokura, K., Wells, D.M., Swarup, K., Yamamoto, M., Mimura, T., Weijers, D., Fukaki, H., Laplace, L., Bennett, M.J., and Guyomarc'h, S. (2016). Quiescent center initiation in the *Arabidopsis* lateral root primordia is dependent on the *SCARECROW* transcription factor. *Development* *143*, 3363–3371.

Hammani, K., and Giegé, P. (2014). RNA metabolism in plant mitochondria. *Trends Plant Sci.* *19*, 380–389.

Heazlewood, J.L., Whelan, J., and Millar, A.H. (2003). The products of the mitochondrial *orf25* and *orfB* genes are Fo components in the plant F1Fo ATP synthase. *Febs Lett.* *540*, 201–205.

Hirayama, T. (2014). A unique system for regulating mitochondrial mRNA poly(A) status and stability in plants. *Plant Signal. Behav.* *9*, e973809.

Hirayama, T., Matsuura, T., Ushiyama, S., Narusaka, M., Kurihara, Y., Yasuda, M., Ohtani, M., Seki, M., Demura, T., Nakashita, H., Narusaka, Y., and Hayashi, S. (2013). A poly(A)-specific ribonuclease directly regulates the poly(A) status of mitochondrial mRNA in *Arabidopsis*. *Nat. Commun.* *4*, 2247.

Hirota, A., Kato, T., Fukaki, H., Aida, M., and Tasaka, M. (2007). The auxin-regulated AP2/EREBP gene PUCHI is required for morphogenesis in the early lateral root primordium of *Arabidopsis*. *Plant Cell* *19*, 2156–2168.

Holec, S., Lange, H., Canaday, J., and Gagliardi, D. (2008). Coping with cryptic and defective transcripts in plant mitochondria. *Biochim. Biophys. Acta* *1779*, 566–573.

Hu, Z.B., Vanderhaeghen, R., Cools, T., Wang, Y., De Clercq, I., Leroux, O., Nguyen, L., Belt, K., Millar, A.H., Audenaert, D., Hilson, P., Small, I., Mouille, G., Vernhettes, S., Van Breusegem, F., Whelan, J., Höfte, H., and De Veylder, L. (2016). Mitochondrial defects confer tolerance against cellulose deficiency. *Plant Cell* *28*, 2276–2290.

Huang, S.B., Van Aken, O., Schwarzländer, M., Belt, K., and Millar, A.H. (2016). The roles of mitochondrial reactive oxygen species in cellular signaling and stress response in plants. *Plant Physiol.* *171*, 1551–1559.

Kanazawa, M., Ikeda, Y., Nishihama, R., Yamaoka, S., Lee, N.H., Yamato, K.T., Kohchi, T., and Hirayama, T. (2020). Regulation of the poly(A) status of mitochondrial mRNA by poly(A)-specific ribonuclease is conserved among land plants. *Plant Cell Physiol.* *61*, 470–480.

- Kobayashi, T., Yagi, Y., and Nakamura, T. (2019). Comprehensive prediction of target RNA editing sites for PLS-class PPR proteins in *Arabidopsis thaliana*. *Plant Cell Physiol.* *60*, 862–874.
- Kohl, M., and Deigner, H.P. (2010). Preprocessing of gene expression data by optimally robust estimators. *BMC Bioinformatics* *11*, 583.
- Konishi, M., and Sugiyama, M. (2003). Genetic analysis of adventitious root formation with a novel series of temperature-sensitive mutants of *Arabidopsis thaliana*. *Development* *130*, 5637–5647.
- Körner, C.G., and Wahle, E. (1997). Poly(A) tail shortening by a mammalian poly(A)-specific 3'-exoribonuclease. *J. Biol. Chem.* *272*, 10448–10456.
- Körner, C.G., Wormington, M., Muckenthaler, M., Schneider, S., Dehlin, E., and Wahle, E. (1998). The deadenylating nuclease (DAN) is involved in poly(A) tail removal during the meiotic maturation of *Xenopus* oocytes. *EMBO J.* *17*, 5427–5437.
- Kwasniak-Owczarek, M., Kazmierczak, U., Tomal, A., MacKiewicz, P., and Janska, H. (2019). Deficiency of mitoribosomal S10 protein affects translation and splicing in *Arabidopsis* mitochondria. *Nucleic Acids Res.* *47*, 11790–11806.
- Lavenus, J., Goh, T., Roberts, I., Guyomarc'h, S., Lucas, M., De Smet, I., Fukaki, H., Beeckman, T., Bennett, M., and Laplace, L. (2013). Lateral root development in *Arabidopsis*: fifty shades of auxin. *Trends Plant Sci.* *18*, 455–463.
- Lee, D., Park, D., Park, J.H., Kim, J.H., and Shin, C. (2019). Poly(A)-specific ribonuclease sculpts the 3' ends of microRNAs. *RNA* *25*, 388–405.
- Lee, H.W., Kim, N.Y., Lee, D.J., and Kim, J. (2009). LBD18/ASL20 regulates lateral root formation in combination with LBD16/ASL18 downstream of ARF7 and ARF19 in *Arabidopsis*. *Plant Physiol.* *151*, 1377–1389.
- Lucas, M., Kenobi, K., Von Wangenheim, D., Voß, U., Swarup, K., De Smet, I., Van Damme, D., Lawrence, T., Péret, B., Moscardi, E., Barbeau, D., Godin, C., Salt, D., Guyomarc'h, S., Stelzer, E.H.K., Maizel, A., Laplace, L., and Bennett, M.J. (2013). Lateral

root morphogenesis is dependent on the mechanical properties of the overlaying tissues. *Proc. Natl. Acad. Sci. U. S. A.* *110*, 5229–5234.

Lupold, S.D., Caoile, A.G.F.S., and Stern, D.B. (1999). Polyadenylation occurs at multiple sites in maize mitochondrial *cox2* mRNA and is independent of editing status. *Plant Cell* *11*, 1565–1577.

Maizel, A., Von Wangenheim, D., Federici, F., Haseloff, J., and Stelzer, E.H.K. (2011). High-resolution live imaging of plant growth in near physiological bright conditions using light sheet fluorescence microscopy. *Plant J.* *68*, 377–385.

Malamy, J.E., and Benfey, P.N. (1997). Organization and cell differentiation in lateral roots of *Arabidopsis thaliana*. *Development* *124*, 33–44.

Murcha, M.W., and Whelan, J. (2015). Isolation of intact mitochondria from the model plant species *Arabidopsis thaliana* and *Oryza sativa*. In *Methods in Molecular Biology*, (Humana Press Inc.), pp. 1–12.

Murphy, E., Vu, L.D., den Broeck, L., Lin, Z.F., Ramakrishna, P., van de Cotte, B., Gaudinier, A., Goh, T., Slane, D., Beeckman, T., Inze, D., Brady, S.M., Fukaki, H., and De Smet, I. (2016). RALFL34 regulates formative cell divisions in *Arabidopsis* pericycle during lateral root initiation. *J. Exp. Bot.* *67*, 4863–4875.

Napsucially-Mendivil, S., Alvarez-Venegas, R., Shishkova, S., and Dubrovsky, J.G. (2014). *ARABIDOPSIS HOMOLOG of TRITHORAX1 (ATX1)* is required for cell production, patterning, and morphogenesis in root development. *J. Exp. Bot.* *65*, 6373–6384.

Ohtani, M., Demura, T., and Sugiyama, M. (2010). Particular significance of SRD2-dependent snRNA accumulation in polarized pattern generation during lateral root development of *Arabidopsis*. *Plant Cell Physiol.* *51*, 2002–2012.

Okushima, Y., Fukaki, H., Onoda, M., Theologis, A., and Tasaka, M. (2007). ARF7 and ARF19 regulate lateral root formation via direct activation of *LBD/ASL* genes in *Arabidopsis*. *Plant Cell* *19*, 118–130.

Otsuka, K. (2012). Studies on mechanisms controlling cell division in the initial stage of lateral root formation with temperature-sensitive mutants of *Arabidopsis*. Doctor thesis. The University of Tokyo.

Otsuka, K., and Sugiyama, M. (2012). Tissue organization of fasciated lateral roots of *Arabidopsis* mutants suggestive of the robust nature of outer layer patterning. *J. Plant Res.* *125*, 547–554.

Otsuka, K., Mamiya, A., Konishi, M., Nozaki, M., Kinoshita, A., Tamaki, H., Arita, M., Saito, M., Yamamoto, K., Hachiya, T., Noguchi, K., Ueda, T., Yagi, Y., Kobayashi, T., Nakamura, T., Sato, Y., Hirayama, T., and Sugiyama, M. (2020). Temperature-dependent fasciation mutants connect mitochondrial RNA processing to the control of cell proliferation during lateral root morphogenesis. *BioRxiv* 2020.06.09.141382.

Pasternak, T., Potters, G., Caubergs, R., and Jansen, M.A.K. (2005). Complementary interactions between oxidative stress and auxins control plant growth responses at plant, organ, and cellular level. *J. Exp. Bot.* *56*, 1991–2001.

Pavlopoulou, A., Vlachakis, D., Balatsos, N.A.A., and Kossida, S. (2013). A comprehensive phylogenetic analysis of deadenylases. *Evol. Bioinforma.* *9*, 491–497.

Planchard, N., Bertin, P., Quadrado, M., Dargel-Graffin, C., Hatin, I., Namy, O., and Mireau, H. (2018). The translational landscape of *Arabidopsis* mitochondria. *Nucleic Acids Res.* *46*, 6218–6228.

Potters, G., Pasternak, T.P., Guisez, Y., and Jansen, M.A.K. (2009). Different stresses, similar morphogenic responses: integrating a plethora of pathways. *Plant Cell Environ.* *32*, 158–169.

Raczynska, K.D., Le Ret, M., Rurek, M., Bonnard, G., Augustyniak, H., and Gualberto, J.M. (2006). Plant mitochondrial genes can be expressed from mRNAs lacking stop codons. *FEBS Lett.* *580*, 5641–5646.

Ramakrishna, P., Duarte, P.R., Rance, G.A., Schubert, M., Vordermaier, V., Vu, L.D., Murphy, E., Barro, A.V., Swarup, K., Moirangthem, K., Jørgensen, B., Van De Cotte, B., Goh, T., Lin, Z., Voß, U., Beeckman, T., Bennett, M.J., Gevaert, K., Maizel, A., and De Smet, I. (2019). EXPANSIN A1-mediated radial swelling of pericycle cells positions

anticlinal cell divisions during lateral root initiation. *Proc. Natl. Acad. Sci. U. S. A.* *116*, 8597–8602.

Reverdatto, S. V., Dutko, J.A., Chekanova, J.A., Hamilton, D.A., and Belostotsky, D.A. (2004). mRNA deadenylation by PARN is essential for embryogenesis in higher plants. *RNA* *10*, 1200–1214.

Sallés, F.J., Richards, W.G., and Strickland, S. (1999). Assaying the polyadenylation state of mRNAs. *Methods-a Companion to Methods Enzymol.* *17*, 38–45.

Shevket, S.H., Gonzalez, D., Cartwright, J.L., Kleanthous, C., Ferguson, S.J., Redfield, C., and Mavridou, D.A.I. (2019). The CcmC-CcmE interaction during cytochrome *c* maturation by System I is driven by protein-protein and not protein-heme contacts. *J. Biol. Chem.* *293*, 16778–16790.

De Smet, I., Vassileva, V., De Rybel, B., Levesque, M.P., Grunewald, W., Van Damme, D., Van Noorden, G., Naudts, M., Van Isterdael, G., De Clercq, R., Wang, J.Y., Meuli, N., Vanneste, S., Friml, J., Hilson, P., Jürgens, G., Ingram, G.C., Inzé, D., Benfey, P.N., and Beeckman, T. (2008). Receptor-like kinase ACR4 restricts formative cell divisions in the *Arabidopsis* root. *Science.* *322*, 594–597.

De Smet, I., Lau, S., Voß, U., Vanneste, S., Benjamins, R., Rademacher, E.H., Schlereth, A., De Rybel, B., Vassileva, V., Grunewald, W., Naudts, M., Levesque, M.P., Ehrismann, J.S., Inzé, D., Luschnig, C., Benfey, P.N., Weijers, D., Van Montagu, M.C.E., Bennett, M.J., Jürgens, G., and Beeckman, T. (2010). Bimodular auxin response controls organogenesis in *Arabidopsis*. *Proc. Natl. Acad. Sci. U. S. A.* *107*, 2705–2710.

Stupar, R.M., Lilly, J.W., Town, C.D., Cheng, Z., Kaul, S., Buell, C.R., and Jiang, J.M. (2001). Complex mtDNA constitutes an approximate 620-kb insertion on *Arabidopsis thaliana* chromosome 2: implication of potential sequencing errors caused by large-unit repeats. *Proc. Natl. Acad. Sci. U. S. A.* *98*, 5099–5103.

Sugimoto, K., Jiao, Y., and Meyerowitz, E.M. (2010). *Arabidopsis* Regeneration from Multiple Tissues Occurs via a Root Development Pathway. *Dev. Cell* *18*, 463–471.

- Sugiyama, M. (2003). Isolation and initial characterization of temperature-sensitive mutants of *Arabidopsis thaliana* that are impaired in root redifferentiation. *Plant Cell Physiol.* *44*, 588–596.
- Swarup, R., Kargul, J., Marchant, A., Zadik, D., Rahman, A., Mills, R., Yemm, A., May, S., Williams, L., Millner, P., Tsurumi, S., Moore, I., Napier, R., Kerr, I.D., and Bennett, M.J. (2004). Structure-function analysis of the presumptive *Arabidopsis* auxin permease AUX1. *Plant Cell* *16*, 3069–3083.
- Takenaka, M., Jörg, A., Burger, M., and Haag, S. (2019). RNA editing mutants as surrogates for mitochondrial SNP mutants. *Plant Physiol. Biochem.* *135*, 310–321.
- Torres-Martínez, H.H., Rodríguez-Alonso, G., Shishkova, S., and Dubrovsky, J.G. (2019). Lateral root primordium morphogenesis in angiosperms. *Front. Plant Sci.* *10*, 206.
- Ulmasov, T., Murfett, J., Hagen, G., and Guilfoyle, T.J. (1997). Aux/IAA Proteins repress expression of reporter genes containing natural and highly active synthetic auxin response elements. *Plant Cell* *9*, 1963–1971.
- Vermeer, J.E.M., von Wangenheim, D., Barberon, M., Lee, Y., Stelzer, E.H.K., Maizel, A., and Geldner, N. (2014). A spatial accommodation by neighboring cells is required for organ initiation in *Arabidopsis*. *Science.* *343*, 178–183.
- Virtanen, A., Henriksson, N., Nilsson, P., and Nissbeck, M. (2013). Poly(A)-specific ribonuclease (PARN): An allosterically regulated, processive and mRNA cap-interacting deadenylase. *Crit. Rev. Biochem. Mol. Biol.* *48*, 192–209.
- von Wangenheim, D., Fangerau, J., Schmitz, A., Smith, R.S., Leitte, H., Stelzer, E.H.K., and Maizel, A. (2016). Rules and self-organizing properties of post-embryonic plant organ cell division patterns. *Curr. Biol.* *26*, 439–449.
- von Wangenheim, D., Hauschild, R., and Friml, J. (2017). Light sheet fluorescence microscopy of plant roots growing on the surface of a gel. *J. Vis. Exp.* *119*, e55044.
- Willems, P., Mhamdi, A., Stael, S., Storme, V., Kerchev, P., Noctor, G., Gevaert, K., and Van Breusegem, F. (2016). The ROS wheel: refining ROS transcriptional footprints. *Plant Physiol.* *171*, 1720–1733.

Figures and tables

(continued on next page)

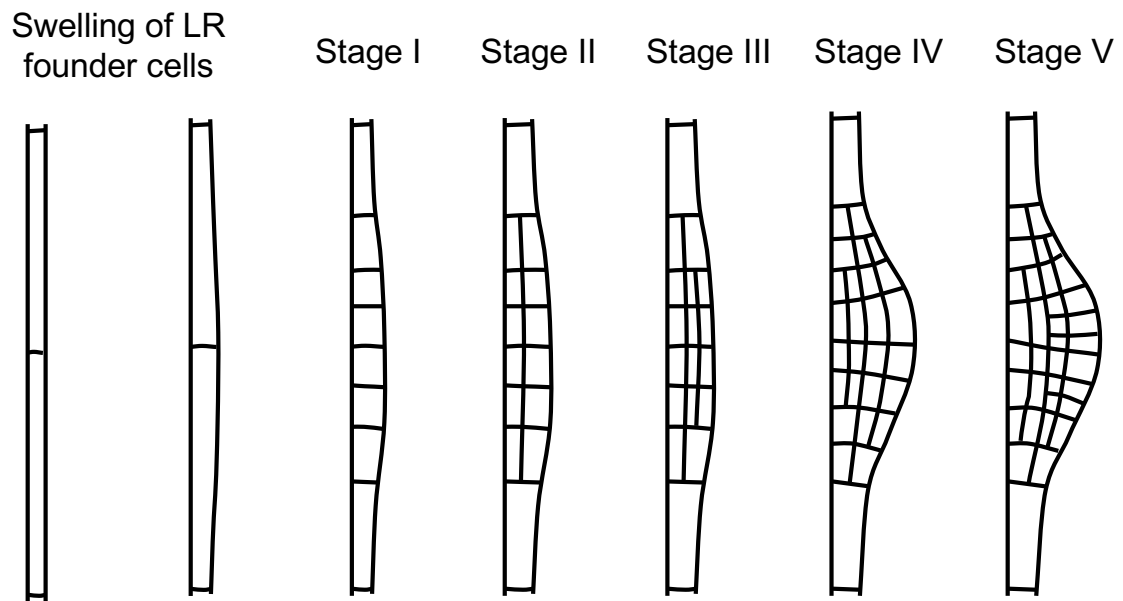


Fig. 1 Schematic of the stages of early LR development in Arabidopsis

A few cells in the xylem pole pericycle layer, termed LR founder cells, undergo radial expansion and subsequently divide in the anticlinal orientation, producing an array of short cells flanked by longer cells, which serve as the origin of the LR primordium (stage I). This is followed by periclinal divisions throughout the primordium, with the exception of the flanking cells in some occasions, creating two cell layers (stage II). Subsequent periclinal cell divisions take place in the central zone of the primordium, producing the third cell layer (stage III), followed by the fourth cell layer (stage IV). The diagram was modified from (Otsuka et al, 2020).

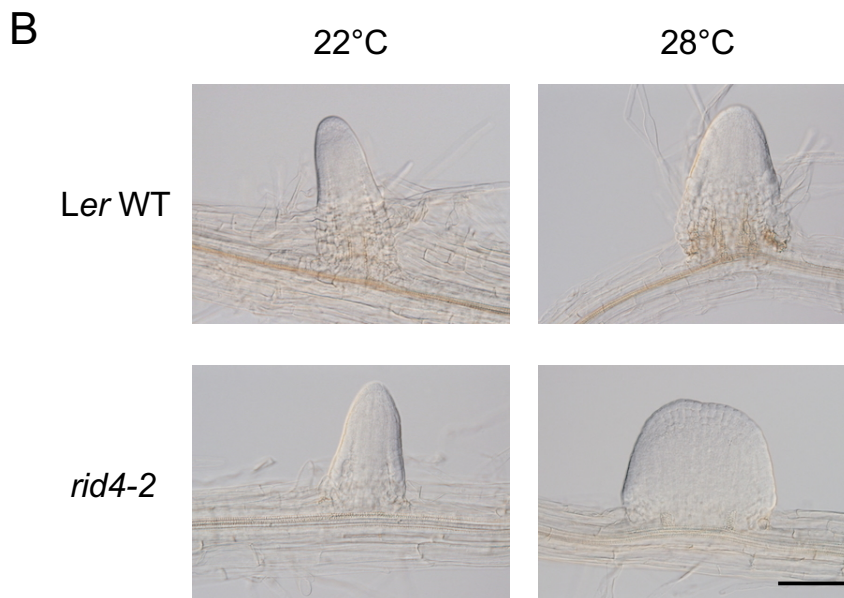
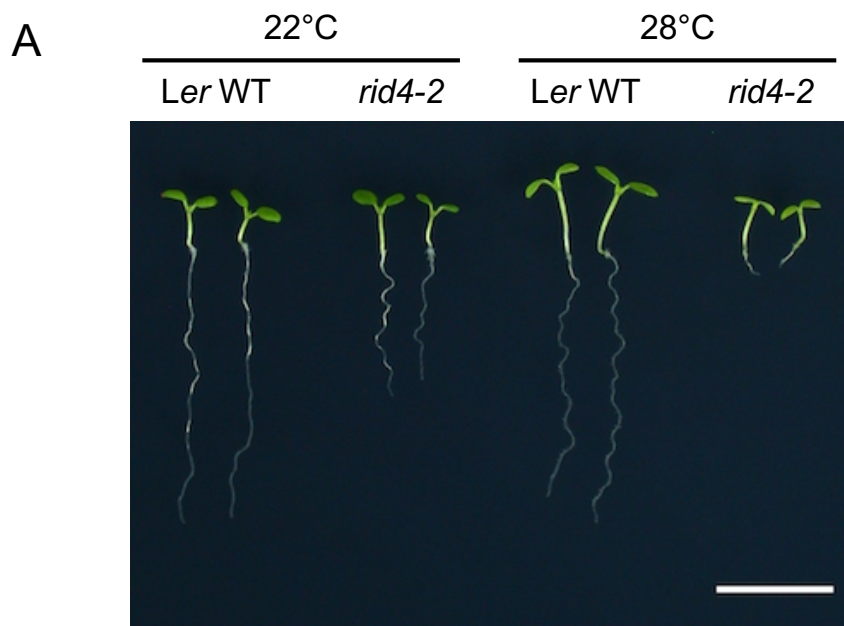


Fig. 2 Temperature-sensitive phenotypes of the TDF mutants exemplified by the *rid4-2* mutant.

(A) Phenotypes of seedlings that were grown for 7 days on vertical agar plates. Seedlings were grown either at 22°C or 28°C. (B) Representative images of LRs formed at 22°C or 28°C in the explants of the wild-type plant or the *rid4-2* mutant after 6 days of culture on indole-3-butyric acid (IBA)-containing medium (RIM). Fasciated LRs were observed in *rid4-2* explants at 28°C. Scale bars, 1 cm (A) and 100 μm (B).

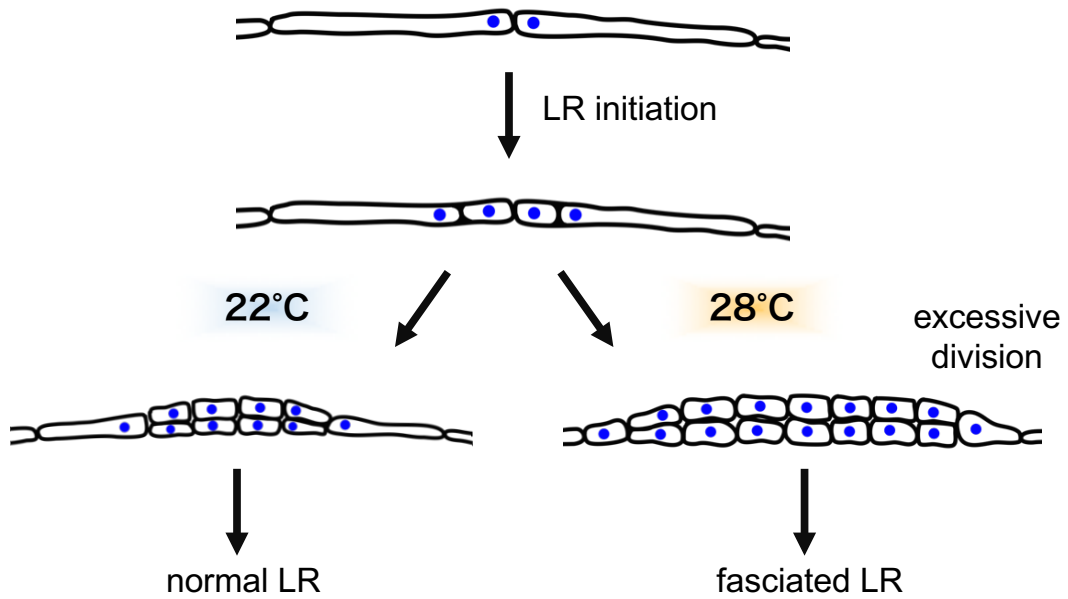


Fig. 3 Schematic of early LR development in the TDF mutants

The TDF mutants form normally-sized LR primordium at permissive temperature (22°C). At non-permissive temperature (28°C), however, excessive cell divisions occur as early as stage II, leading to the formation of fasciated LR (Otsuka, 2012; Otsuka et al., 2020).

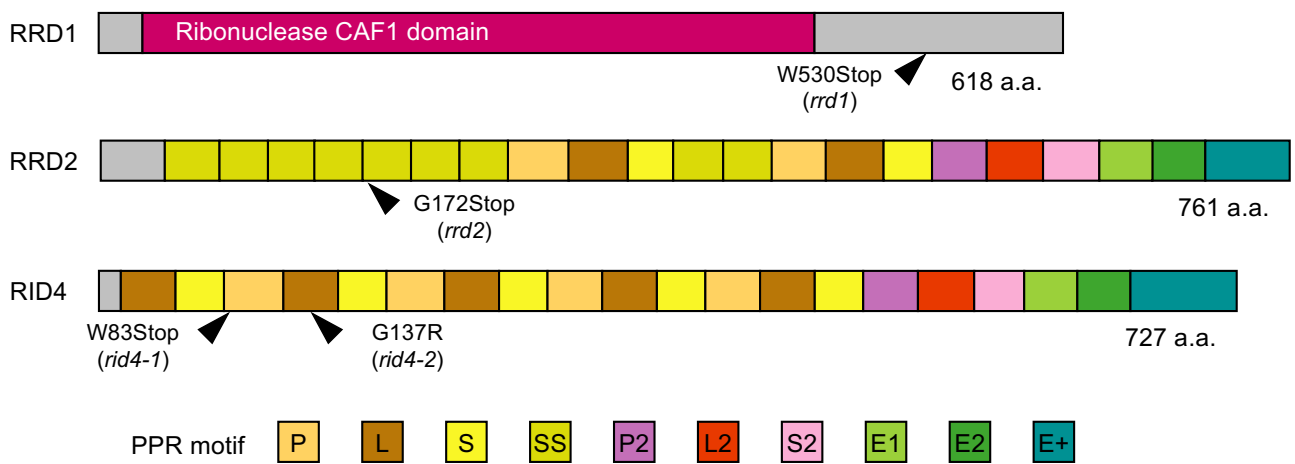


Fig. 4 The structure of the TDF proteins

RRD1 (At3g25430) encodes a poly(A)-specific ribonuclease (PARN)-like protein. *RRD2* (At1g32415) and *RID4* (At2g33680) both encode a pentatricopeptide repeat (PPR) protein belonging to the PLS subfamily. The position of each TDF mutation is indicated by black arrowheads. The diagrams were modified from (Otsuka, 2012). The PPR motifs of *RRD2* and *RID4* were depicted based on a recent study (Cheng et al., 2016). Scale bar, 100 amino acids (a. a.).

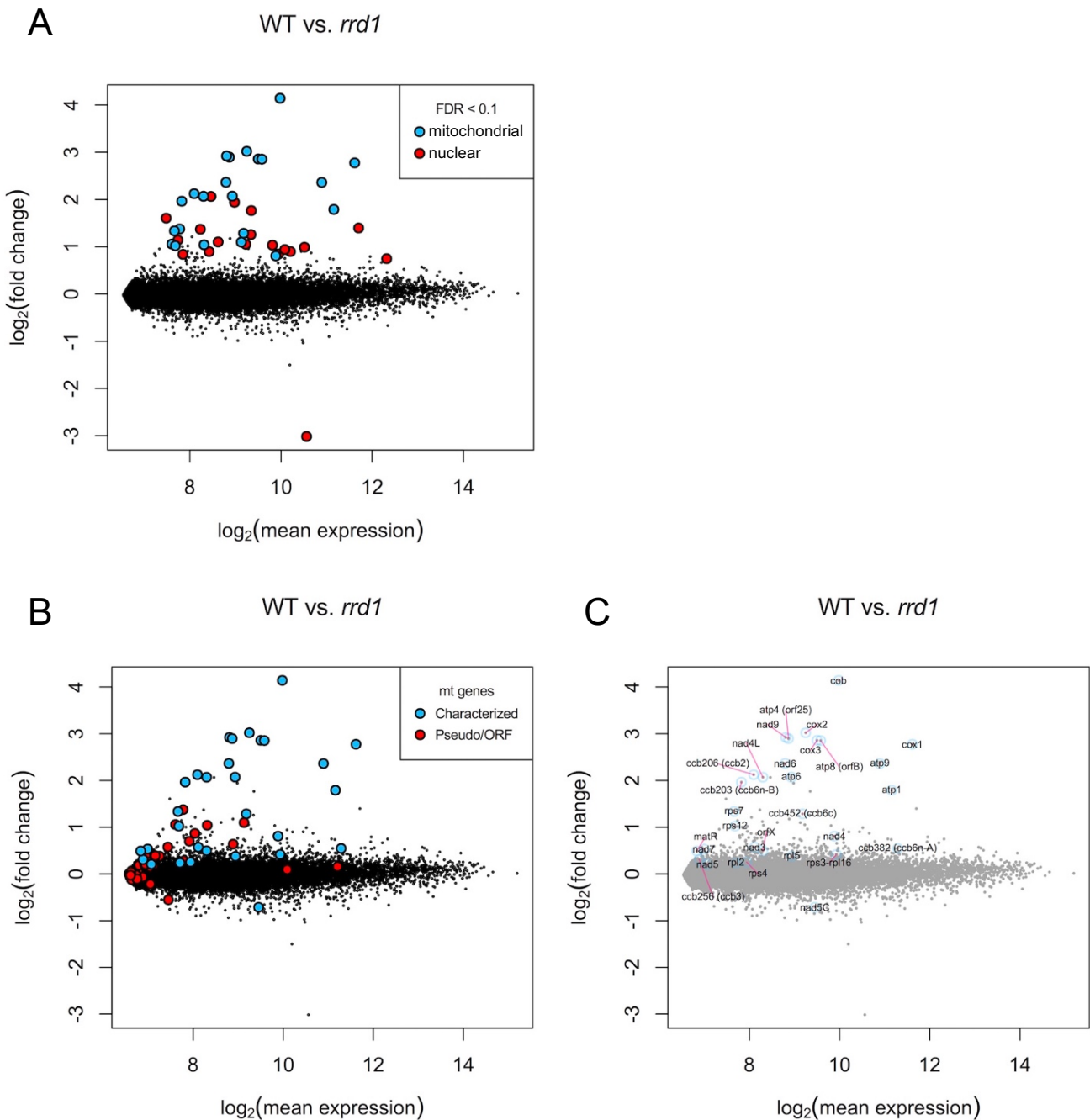


Fig. 5 Microarray analysis of gene expression in *rrd1*

(A–C) MA plot for the microarray analysis of poly(A)⁺ transcripts of *rrd1* vs. wild-type (WT) explants in which LR_s were induced at 28°C for 12 hours. Genes are plotted according to their fold change (*rrd1*/WT) and mean expression between *rrd1* and the WT. (A) Differentially expressed genes (FDR < 0.1) are highlighted. Mitochondrial genes are shown in blue, while nuclearly-encoded genes are shown in red. (B) The functionally characterized mitochondrial genes are shown in blue, while the non-characterized mitochondrial ORFs or pseudogenes are shown in red. (C) The names of the functionally characterized mitochondrial genes are shown.

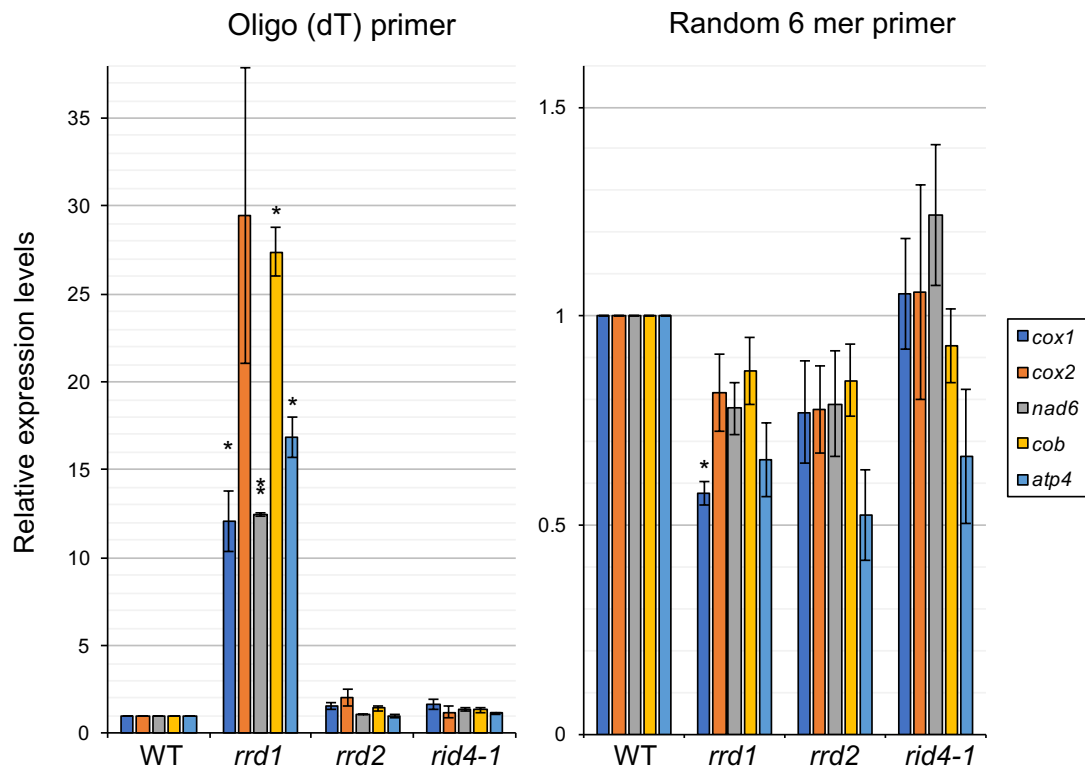


Fig. 6 qRT-PCR analysis of mitochondrial transcripts in the TDF mutants

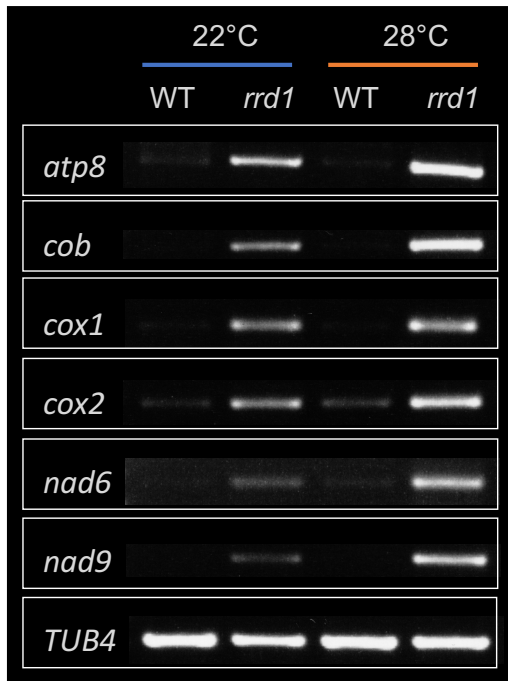
qRT-PCR analysis of explants in which LRs were induced at 28°C for 12 hours. The levels of total (reverse transcribed with random 6 mer primer; right panel) and polyadenylated (reverse transcribed with oligo (dT) primer; left panel) transcripts are shown for *cytochrome oxidase subunit 1 (cox1)*, *cox2*, *NADH dehydrogenase subunit 6 (nad6)*, *apocytochrome B (cob)*, and *ATP synthase subunit 4 (atp4)* (mean \pm s.d., N = 3, * P < 0.05, ** P < 0.01, Welch's t test with Benjamini-Hochberg correction).

WT	<i>rrd1</i>
GAACTTTTAGAAATTTATGCATGGTTATCT	GAACTTTTAGAAATTTATGCATGGTTATCT
#1 GAACUUUUAGAAUUUAUGCAAAAAAAAAA	#1 GAACUUCUAGAAUUUUAU
#2 GAACUUUUAAA	#2 GAACUUUUAGAAUUUA
#3 GAACUUUUAA	#3 GAACUUUUAGAAUUUA
#4 GAACUUUUA	#4 GAACUUUUAGAAUU
#5 GAACUUUUA	#5 GAACUUUUAGAAAACAAAAAAAAAAAAAAAAAAAA
#6 GAACUUUU	#6 GAACUUUUAGAAAACAAAAAAAAAAAAAAAAAAAA
#7 GAACUUUU	#7 GAACUUUUAGAAAAAAAAAAAAAAAAAAAAAAA
#8 GAACUUUU	#8 GAACUUUUAGAAAAAAAAAAAAAAAAAAAAAAA
#9 GAACUUUU	#9 GAACUUUUAGAAAAAAAAAAAAAAAAAAAAAAA
#10 GAACUUUU	#10 GAACUCUUAGAAAAAAA
#11 GAACUUUU	#11 GAACUUUUAGAAAAA
#12 GAACUUUU	#12 GAACUUUUAGAAAA
#13 GAACUUUU	#13 GAACUUUUAGAAAA
#14 GAACUUUU	#14 GAACUUUUAGAAA
#15 GAACUUUU	#15 GAACUUUUAGAA
#16 GAACUUUU	#16 GAACUUUUACAA
#17 GAACUUUU	#17 GAACUUUUAG
#18 GAACUUUU	#18 GAACUUUUAG
#19 GAACUUUU	#19 GAACUUUUAA
#20 GAACUCUU	#20 GAACUUUUAA
#21 GAACUUUAA	#21 GAACUUUUA
#22 GAACUUUAA	#22 GNAACUAAAAAAAAAAAAAAAAACAAA
#23 GAACUUUA	
#24 GAACUUU	

Fig. 7 CR-RT PCR analysis of *cox1* transcripts in *rrd1*

Analysis of the 3' end of the *cox1* mRNA by CR-RT PCR. mRNAs were prepared from WT and *rrd1* seedlings that were first grown at 22°C for 7 days, and then at 28°C for 2 days. The genomic sequence of *cox1* is shown in green.

A



B

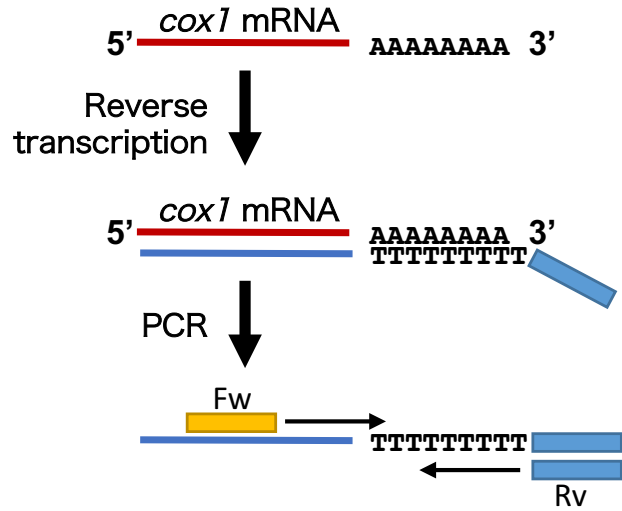


Fig. 8 RACE-PAT assay of mitochondrial transcripts in *rrd1*

(A) RACE-PAT assay showing the accumulation of polyadenylated transcripts of *atp8*, *cob*, *cox1*, *cox2*, *nad6*, *nad9*, and *TUB4*. mRNAs were prepared from explants in which LR_s were induced at 22°C or 28°C for 12 hours. (B) Schematic of the principles of the RACE-PAT assay.

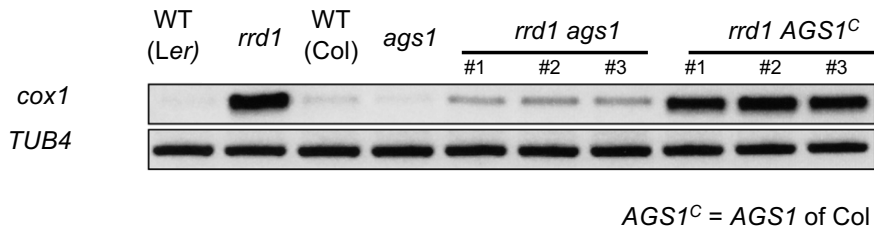
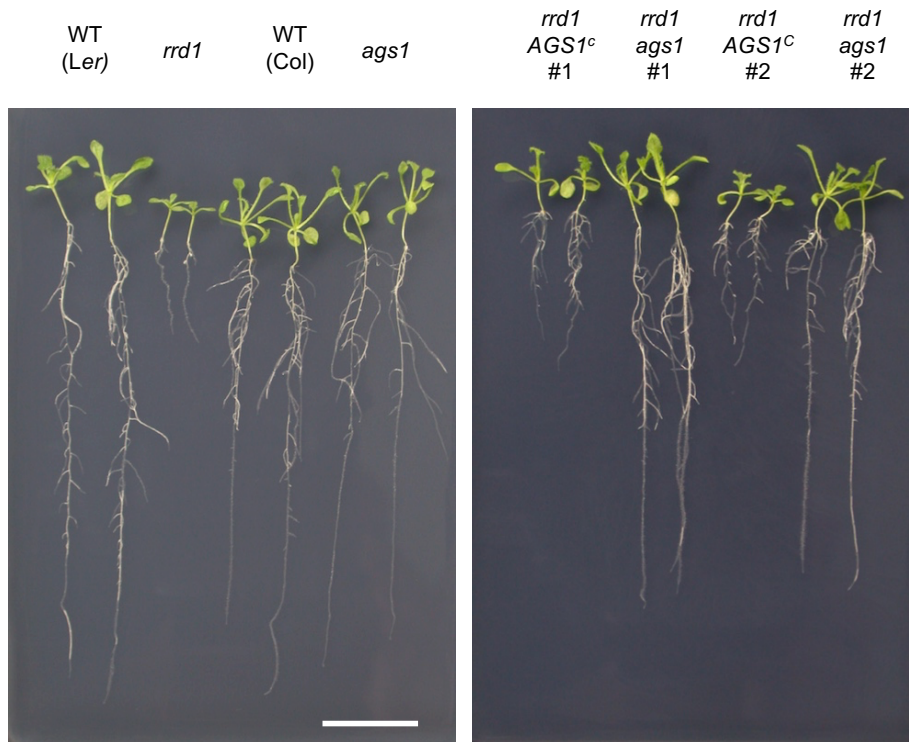
A**B**

Fig. 9 Effects of the introduction of *ags1* into *rrd1*.

(A) RACE-PAT assay showing the accumulation of polyadenylated transcripts of *cox1* and *TUB4*. *rrd1* mutant strains harboring either *ags1* or *AGS1^c* (*AGS1* of Col background) were obtained by *rrd1* (*Ler* background) × *ags1* (Col background) and *rrd1* × Col crosses, respectively. mRNAs were prepared from seedlings that were first grown at 22°C for 5 days, and then at 28°C for 3 days. (B) Seedlings grown at 28°C for 13 days on gellan gum plates. Scale bar, 2 cm (B).

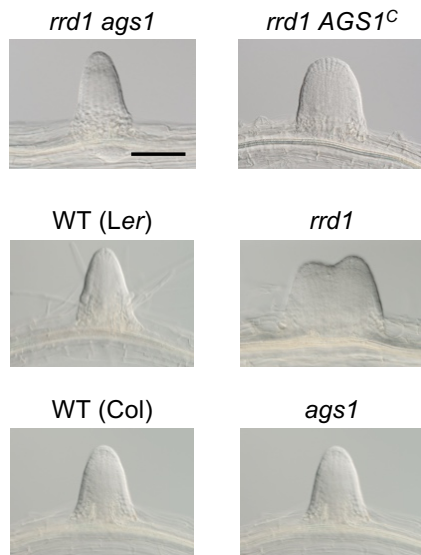
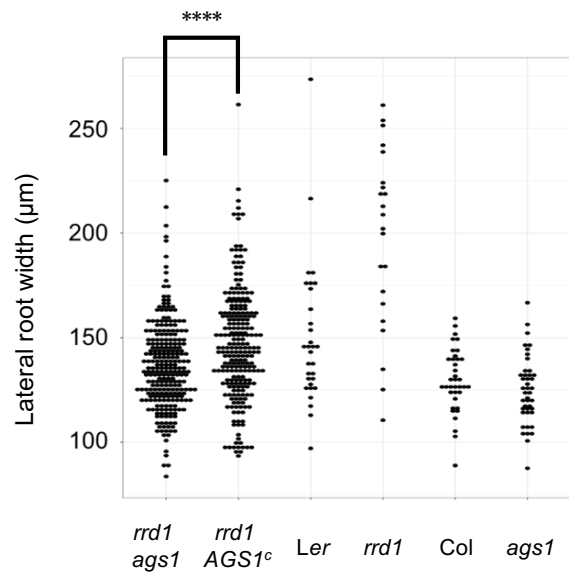
A**B**

Fig. 10 Effects of *ags1* on the LR fasciation phenotype of *rrd1*.

(A) Representative images of LRs formed at 28°C after 6 days of culture. **(B)** The basal width of the LRs that were formed as in (A) was scored (lower panel, N = 115–116 for *rrd1*, *ags1*, and *rrd1 AGS1^c*, N = 22–43 for others, **** $P < 10^{-4}$, Mann–Whitney–Wilcoxon test with Bonferroni correction).

<i>atp1</i>		1110	1178	1292	1415	1484																		
	LerWT	-0.36	0.49	0.49	0.49	0.50																		
	<i>rrd2</i>	-0.40	0.49	0.49	0.46	0.50																		
	<i>rid4-1</i>	-0.42	0.48	0.47	0.46	0.50																		
<i>atp4</i>		89	138	215	248	250	251	382	395	416														
	LerWT	-0.23	0.31	0.50	0.45	0.10	0.48	-0.40	0.50	0.47														
	<i>rrd2</i>	-0.24	0.32	0.50	0.47	0.12	0.49	-0.45	0.48	0.46														
	<i>rid4-1</i>	-0.31	0.25	0.48	0.46	0.04	0.47	-0.42	-0.48	0.45														
	<i>rid4-2</i>	-0.31	0.22	0.48	0.45	-0.04	0.48	-0.41	-0.28	0.47														
<i>atp6</i>		475																						
	LerWT	0.46																						
	<i>rrd2</i>	0.43																						
	<i>rid4</i>	0.42																						
<i>atp9</i>		53	83	167	224																			
	LerWT	0.46	0.49	0.48	0.46																			
	<i>rrd2</i>	0.46	0.47	0.48	0.46																			
	<i>rid4-1</i>	0.44	0.47	0.45	0.45																			
<i>ccb2</i>		16	28	71	75	78	80	128	137	148	149	154	159	160	164	172	179	181	188	193	194			
	LerWT	-0.04	0.09	0.01	-0.48	-0.49	-0.06	0.03	0.04	0.04	0.01	0.00	0.04	0.10	0.02	0.12	0.01	0.01	-0.48	-0.02	0.00			
	<i>rrd2</i>	-0.19	-0.22	-0.45	-0.50	-0.50	-0.29	-0.22	-0.23	-0.25	-0.26	-0.26	-0.24	-0.24	-0.22	-0.21	-0.21	-0.22	-0.48	-0.25	-0.31			
	<i>rid4-1</i>	-0.28	-0.36	-0.31	-0.50	-0.50	-0.38	-0.28	-0.33	-0.36	-0.36	-0.37	-0.36	-0.35	-0.35	-0.33	-0.36	-0.35	-0.48	-0.37	-0.41			
<i>ccb2</i>		286	304	338	367	379	380	406	424	428	467	475	476	485	512	514	551	554	566	569				
	LerWT	0.03	0.03	0.01	0.00	-0.04	0.02	-0.42	-0.01	-0.02	-0.06	0.02	0.01	0.02	-0.05	0.00	0.01	0.00	-0.02	0.03				
	<i>rrd2</i>	-0.19	-0.24	-0.20	-0.23	-0.25	-0.21	-0.45	-0.26	-0.23	-0.27	-0.21	-0.22	-0.21	-0.29	-0.24	-0.23	-0.27	-0.25	-0.21				
	<i>rid4-1</i>	-0.39	-0.38	-0.35	-0.39	-0.40	-0.37	-0.47	-0.40	-0.39	-0.40	-0.39	-0.39	-0.38	-0.45	-0.38	-0.38	-0.41	-0.40	-0.42				
<i>ccb3</i>		103	133	179	184	262	331	395	400	421	436	446	458	463	467	473	477	497	521	548	568			
	LerWT	0.26	0.22	0.22	0.23	-0.46	0.27	0.25	0.21	0.25	0.24	0.28	0.28	0.27	0.28	0.31	-0.48	0.34	0.33	0.35	0.32			
	<i>rrd2</i>	-0.37	-0.18	-0.25	-0.37	-0.50	-0.23	-0.28	-0.23	-0.28	-0.21	-0.24	-0.22	-0.27	-0.26	-0.27	-0.45	-0.24	-0.27	-0.38	-0.24			
	<i>rid4-1</i>	-0.39	-0.28	-0.26	-0.40	-0.47	-0.27	-0.31	-0.33	-0.26	-0.28	-0.25	-0.28	-0.30	-0.28	-0.27	-0.50	-0.30	-0.26	-0.28	-0.27			
<i>ccb3</i>		575	608	614	618	619	624	650	656	673														
	LerWT	0.36	0.37	0.34	0.40	0.37	0.02	0.38	0.39	0.20														
	<i>rrd2</i>	-0.43	-0.31	-0.30	-0.36	-0.31	-0.45	-0.41	-0.33	-0.40														
	<i>rid4-1</i>	-0.28	-0.31	-0.30	-0.39	-0.32	-0.50	-0.39	-0.31	-0.43														
<i>ccb6c</i>		50	103	122	123	146	155	160	175	333	334	378	406	415	561	925	1150	1172	1215	1246	1280	1327		
	LerWT	0.44	0.46	0.48	0.46	0.46	0.49	0.39	0.29	0.42	0.50	-0.19	0.48	0.48	-0.44	-0.35	-0.48	0.42	-0.03	0.37	0.45	0.31		
	<i>rrd2</i>	0.47	0.48	0.50	0.43	0.47	0.50	0.41	0.23	0.38	0.50	0.01	0.50	0.39	-0.33	-0.50	-0.47	0.47	-0.06	0.28	0.48	0.48		
	<i>rid4-1</i>	0.47	0.49	0.50	0.28	0.48	0.48	0.43	0.21	0.27	0.50	-0.14	0.50	0.39	-0.37	-0.43	-0.45	0.47	-0.08	0.34	0.42	0.50		
<i>ccb6n-A</i>		44	104	143	157	200	262	269	289	340	371	378	404	484	579	581	709	710	719	779	791	806	955	
	LerWT	0.37	0.48	0.39	0.38	-0.48	0.48	0.43	0.41	-0.47	-0.44	0.37	-0.40	-0.45	-0.48	-0.50	0.01	0.42	-0.48	0.47	0.42	0.45	0.47	
	<i>rrd2</i>	0.35	0.47	0.35	0.36	-0.48	0.47	0.42	0.39	-0.47	-0.43	0.35	-0.38	-0.46	-0.50	-0.48	-0.03	0.39	-0.48	0.46	0.39	0.45	0.45	
	<i>rid4-1</i>	0.30	0.46	0.38	0.31	-0.48	0.40	0.42	0.37	-0.47	-0.45	0.35	-0.38	-0.45	-0.50	-0.48	-0.16	0.37	-0.49	0.47	0.41	0.43	0.47	
<i>ccb6n-B</i>		65	176	208	226	259	277	301	320	344	356	391	467											
	LerWT	0.41	0.40	0.37	0.36	0.32	0.34	-0.49	0.09	0.30	0.29	0.35	-0.48											
	<i>rrd2</i>	0.29	0.37	0.27	0.28	0.22	0.24	-0.49	0.03	0.23	0.19	0.29	-0.50											
	<i>rid4-1</i>	0.23	0.34	0.21	0.20	0.16	0.19	-0.48	-0.01	0.15	0.12	0.23	-0.50											
<i>cob</i>		118	286	325	568	610	853	908	924	982	1084													
	LerWT	0.48	0.48	0.43	0.45	-0.28	0.50	0.50	-0.38	0.50	0.50													
	<i>rrd2</i>	0.48	0.49	0.49	0.48	-0.26	0.41	0.50	-0.37	0.41	0.46													
	<i>rid4-1</i>	0.46	0.48	0.42	0.46	-0.26	0.42	0.41	-0.33	0.38	0.48													
<i>cox2</i>		24	25	27	71	138	253	261	278	379	476	557	581	698	721	742								
	LerWT	-0.43	-0.04	0.40	0.46	-0.02	0.49	-0.46	0.50	0.50	0.50	0.48	0.39	0.50	0.47	-0.44								
	<i>rrd2</i>	-0.39	-0.05	0.42	0.49	0.03	0.50	-0.45	0.50	0.47	0.50	0.50	0.41	0.50	0.45	-0.50								
	<i>rid4-1</i>	-0.39	-0.02	0.38	0.46	0.10	0.50	-0.45	0.50	0.50	0.50	0.50	0.45	0.50	0.49	-0.49								
<i>cox3</i>		112	245	257	311	314	413	422	603															
	LerWT	0.50	0.48	0.50	0.50	0.48	0.50	0.46	-0.50															
	<i>rrd2</i>	0.50	0.50	0.47	0.50	0.50	0.50	0.50	-0.50															
	<i>rid4-1</i>	0.50	0.50	0.46	0.46	0.44	0.30	0.29	-0.28															

$$\text{Editing status} = U / (C+U) - 0.5$$



Fig. 11 Comprehensive analysis of mitochondrial mRNA editing in *rrd2* and *rid4-1*.

(continued on next page, legend follows)

<i>mat R</i>		80	241	284	374	461	1593	1596	1676	1730	1731	1751	1771	1807	1895							
	LerWT	-0.46	-0.46	-0.49	0.48	0.47	-0.21	-0.32	-0.47	0.36	0.12	0.35	0.31	0.21	0.41							
	<i>rrd2</i>	-0.48	-0.46	-0.49	0.43	0.44	-0.19	-0.33	-0.47	0.36	0.14	0.34	0.27	0.19	0.40							
	<i>rid4-1</i>	-0.48	-0.46	-0.48	0.42	0.44	-0.29	-0.39	-0.46	0.32	0.04	0.30	0.28	0.15	0.38							
<i>nad1a</i>		2	167	265	307	308	376															
	LerWT	0.47	0.50	0.47	0.50	0.50	0.48															
	<i>rrd2</i>	0.49	0.45	0.45	0.45	0.45	0.48															
	<i>rid4-1</i>	0.42	0.43	0.45	0.45	0.44	0.48															
<i>nad1b</i>		490	492	493	500	536	546	571	580	635												
	LerWT	0.50	0.45	0.44	0.50	0.50	-0.50	0.47	0.50	0.50												
	<i>rrd2</i>	0.50	0.50	0.50	0.34	0.50	-0.50	0.44	0.46	0.31												
	<i>rid4-1</i>	0.50	0.50	0.50	0.23	0.50	-0.50	0.45	0.43	0.41												
<i>nad1c</i>		674	725	743	755	763	797	823	898	928	937											
	LerWT	0.48	0.47	0.50	0.50	-0.50	-0.50	0.50	0.50	0.48	0.47											
	<i>rrd2</i>	0.49	0.46	0.50	0.50	-0.50	-0.50	0.50	0.50	0.50	0.48											
	<i>rid4-1</i>	0.48	0.50	0.50	0.50	-0.50	-0.50	0.50	0.50	0.48	0.47											
<i>nad2a</i>		28	59	89	90	285	341	344	389	394	400	427	441	461	528	530	558					
	LerWT	0.42	0.48	0.45	0.26	-0.40	0.50	0.50	0.44	0.46	0.50	0.50	-0.50	0.44	-0.50	0.50	-0.50					
	<i>rrd2</i>	0.44	0.48	0.48	0.23	-0.35	0.50	0.47	0.44	0.47	0.50	0.50	-0.50	0.47	-0.50	0.50	-0.40					
	<i>rid4-1</i>	0.45	0.48	0.46	0.24	-0.34	0.47	0.50	0.41	0.47	0.46	0.50	-0.42	0.47	-0.38	0.50	-0.45					
<i>nad2b</i>		642	695	821	842	953	961	991	995	1091	1160	1233	1279	1280	1309	1433	1436	1490				
	LerWT	-0.46	0.50	0.50	0.50	0.50	0.50	0.50	0.50	0.50	0.50	-0.42	0.45	0.46	0.50	0.50	0.50	-0.42				
	<i>rrd2</i>	-0.44	0.50	0.50	0.50	0.50	0.50	0.50	0.50	0.50	0.50	-0.39	0.50	0.50	0.50	0.50	0.50	-0.45				
	<i>rid4-1</i>	-0.44	0.50	0.50	0.50	0.50	0.50	0.50	0.50	0.50	0.50	-0.43	0.50	0.50	0.50	0.50	0.50	-0.40				
<i>nad3</i>		8	26	64	69	83	149	211	212	250	254	347	352									
	LerWT	-0.44	0.46	0.40	-0.49	0.35	0.36	0.31	0.38	0.29	0.30	-0.46	-0.46									
	<i>rrd2</i>	-0.36	0.45	0.27	-0.46	0.30	0.32	0.25	0.31	0.21	0.26	-0.46	-0.43									
	<i>rid4-1</i>	-0.25	0.40	0.19	-0.48	0.21	0.24	0.15	0.22	0.11	0.13	-0.47	-0.30									
<i>nad4</i>		29	74	84	107	124	158	164	166	197	317	362	376	402	403	418	436	437	449	608	659	
	LerWT	0.45	0.43	-0.45	0.45	0.48	0.44	0.46	0.43	0.47	0.49	0.44	0.50	-0.50	0.50	-0.50	0.50	0.50	0.50	0.45	0.50	0.50
	<i>rrd2</i>	0.45	0.36	-0.33	0.50	0.50	0.50	0.45	0.46	0.50	0.50	0.50	0.50	-0.50	0.50	-0.50	0.50	0.50	0.50	0.50	0.50	0.50
	<i>rid4-1</i>	0.50	0.43	-0.30	0.50	0.50	0.50	0.47	0.47	0.47	0.50	0.50	0.50	-0.50	0.31	-0.50	0.50	0.50	0.50	0.50	0.50	0.40
<i>nad4L</i>		767	784	836	896	977	1010	1033	1101	1129	1131	1133	1148	1172	1206	1355	1373	1401	1405	1417	1433	
	LerWT	0.45	0.44	0.50	0.50	0.46	0.50	0.49	-0.01	0.48	-0.39	-0.40	0.45	0.46	-0.46	0.45	0.44	-0.41	0.39	0.50	0.45	
	<i>rrd2</i>	0.50	0.50	0.50	0.50	0.47	0.46	0.49	0.19	0.48	-0.28	-0.29	0.50	0.50	-0.47	0.50	0.45	-0.44	0.50	0.50	0.50	
	<i>rid4-1</i>	0.46	0.46	0.50	0.50	0.50	0.50	0.50	0.13	0.50	-0.47	-0.49	0.50	0.50	-0.47	0.50	0.50	-0.50	0.50	0.50	0.43	
<i>nad4L</i>		41	55	86	95	100	110	131	158	188	197											
	LerWT	0.50	0.48	0.46	0.48	0.46	0.50	0.43	0.48	0.46	0.44											
	<i>rrd2</i>	0.50	0.50	0.47	0.44	0.44	0.49	0.43	0.48	0.42	0.45											
	<i>rid4-1</i>	0.50	0.50	0.47	0.42	0.44	0.46	0.37	0.44	0.40	0.41											
<i>nad5a</i>		155	242	272	358	374	398	494	548	553	598	608	609	629	676	713	725	764	835	863	875	1275
	LerWT	0.50	0.41	0.41	0.50	0.47	0.47	0.48	0.49	0.49	0.49	0.47	0.25	0.50	0.50	0.50	0.49	0.50	0.48	0.50	0.50	0.50
	<i>rrd2</i>	0.50	0.44	0.39	0.50	0.49	0.50	0.50	0.48	0.48	0.50	0.47	0.33	0.50	0.50	0.50	0.50	0.48	0.50	0.48	0.47	0.46
	<i>rid4-1</i>	0.50	0.48	0.39	0.50	0.48	0.50	0.50	0.49	0.50	0.50	0.50	0.34	0.50	0.50	0.50	0.48	0.48	0.48	0.50	0.50	0.50
<i>nad5c</i>		1490	1550	1580	1610	1665	1731	1895	1916	1918	1929	1958										
	LerWT	0.46	0.48	0.47	0.46	-0.29	-0.39	0.49	0.50	0.47	-0.40	-0.48										
	<i>rrd2</i>	0.45	0.45	0.46	0.46	-0.31	-0.44	0.50	0.50	0.50	-0.40	-0.50										
	<i>rid4-1</i>	0.44	0.44	0.50	0.45	-0.30	-0.43	0.50	0.50	0.50	-0.36	-0.45										
<i>nad7</i>		24	38	77	137	200	209	213	244	251	316	335	344	578	679	698	724	734	739	769	789	
	LerWT	0.44	0.50	0.50	0.50	0.50	0.50	0.14	0.50	0.50	0.50	0.50	0.50	0.50	0.50	0.50	0.50	0.50	0.50	0.50	0.50	-0.40
	<i>rrd2</i>	0.50	0.50	0.50	0.50	0.50	0.50	0.15	0.50	0.50	0.50	0.50	0.50	0.50	0.50	0.50	0.50	0.50	0.50	0.50	0.50	-0.40
	<i>rid4-1</i>	0.45	0.50	0.50	0.50	0.50	0.50	0.13	0.50	0.50	0.50	0.50	0.50	0.50	0.50	0.50	0.50	0.50	0.50	0.50	0.50	-0.41
<i>nad7</i>		795	926	963	1050	1057	1079	1082	1088	1103	1124	1137										
	LerWT	-0.16	0.50	0.50	-0.40	0.50	0.44	-0.50	0.45	0.50	0.50	-0.03										
	<i>rrd2</i>	-0.18	0.50	0.44	-0.37	0.50	0.50	-0.45	0.50	0.50	0.50	0.05										
	<i>rid4-1</i>	-0.20	0.50	0.46	-0.37	0.50	0.50	-0.46	0.50	0.50	0.50	0.04										

Editing status = $U / (C+U) - 0.5$

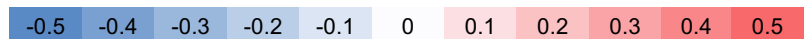
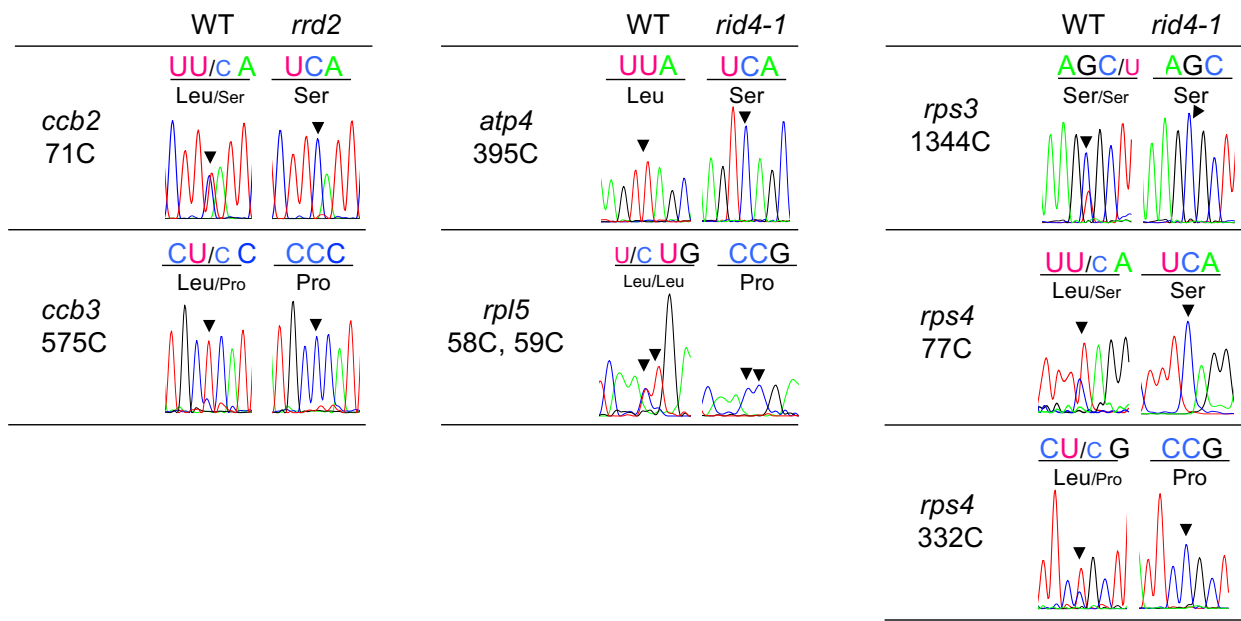


Fig. 11 Comprehensive analysis of mitochondrial mRNA editing in *rrd2* and *rid4-1*.

(continued on next page, legend follows)

A



B

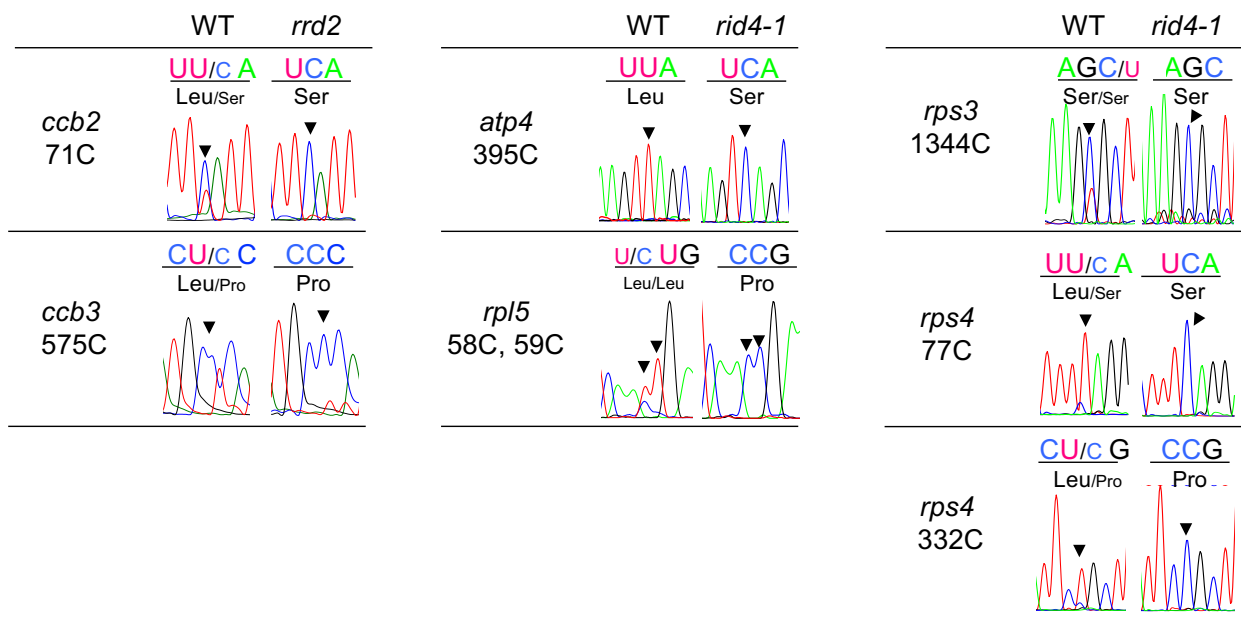
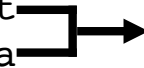


Fig. 12 Editing sites severely affected by *rrd2* and *rid4*

Sequencing analysis of mitochondrial mRNA editing in explants in which LR_s were induced at 28°C (**A**) or at 22°C (**B**) for 12 hours. Black arrows indicate the editing sites. The codon located at the editing site is shown above.

Estimated binding sites of RRD2

ccb2	71C	accaat cacgag tttt t		8/17 match (P = 2.79 x 10 ⁻²)
ccb3	575C	atcaat acatg ttt cta		
ccb3	624C	tt cct tcttcttaact tg		

Estimated binding sites of RID4

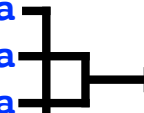
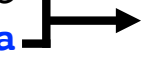
atp4	395C	ccg aa act t aaatg t ta		12/17 match (P = 9.75 x 10 ⁻⁵)
rpl5	59C	tca ag at t g tt g t ca		
rps3	1344C	ata aa at t g ttt at ca		
rps4	77C	tca aa ctt g tcg t ac		
rps4	332C	aac aa gat t gacg t ta		9/17 match (P = 9.28 x 10 ⁻³)
ccb3	624C	ttcctcttcttaact tg		

Fig. 13 Analysis of estimated binding sites of RRD2 and RID4

Alignment of the estimated binding sequence of RRD2 and RID4 for each editing site is shown. The sequence data was extracted from (Kobayashi et al., 2019).

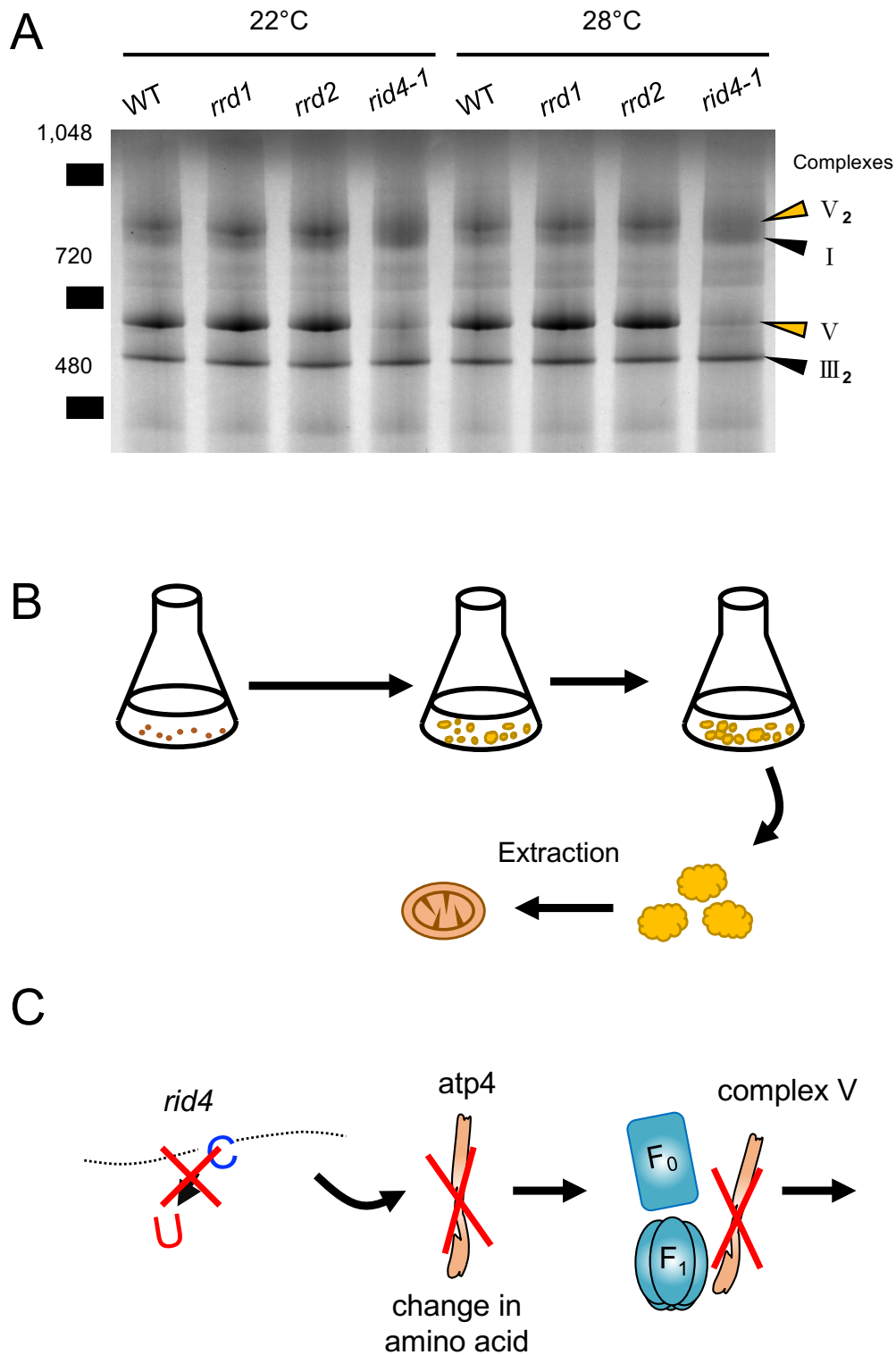


Fig. 14 Analysis of mitochondrial respiratory chain complexes in the TDF mutants

(A) BN-PAGE analysis of mitochondrial protein complexes. Mitochondria were extracted from seed-derived liquid-cultured callus that were first incubated at 22°C for 20 days, and then at 22°C or 28°C for an additional 3 days. (B) Schematic depicting the callus culture used in mitochondrial extraction. (C) Schematic of the effects of *rid4* on complex V biosynthesis.

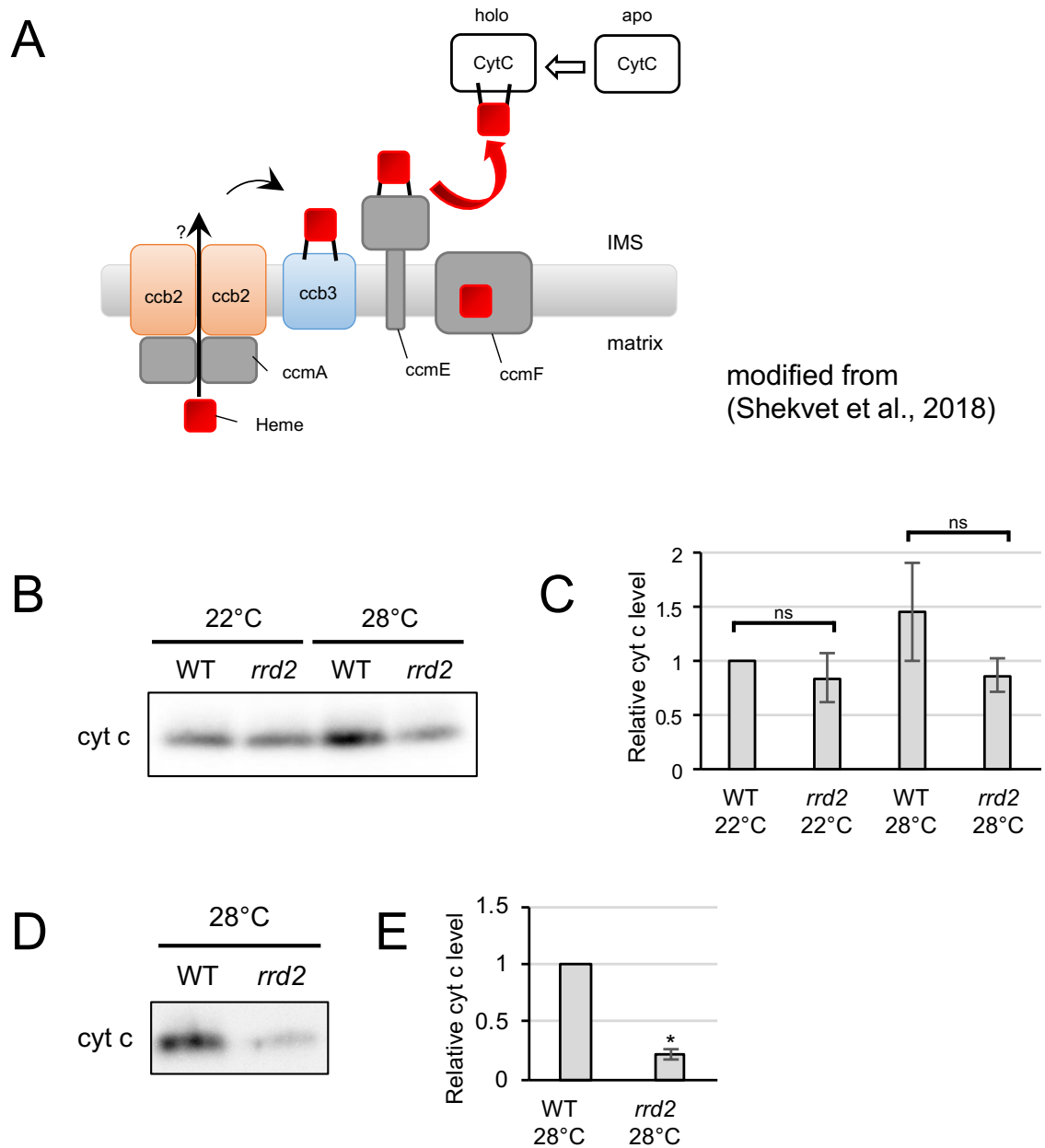


Fig. 15 Analysis of cytochrome c biogenesis in *rrd2*

(A) Schematic of the cytochrome *c* maturation pathway in plant mitochondria. **(B and C)** Immunoblot analysis of cyt *c*. Mitochondria were extracted in the same conditions as in Fig. 14. The results of the densitometry analysis are shown in **(C)** (N = 3, mean ± s.d.). **(D and E)** Immunoblot analysis of cyt *c* using mitochondria extracted from callus that were cultured first at 22°C for 14 days, and then at 28°C for 7 days. The results of the densitometry analysis are shown in **(E)** (N = 2, mean ± s.d., ** $P < 0.01$, Welch's *t* test)

Fig.16 については5年以内に雑誌等で刊行予定のため、非公開。

Fig.17 については5年以内に雑誌等で刊行予定のため、非公開。

Fig.18 については5年以内に雑誌等で刊行予定のため、非公開。

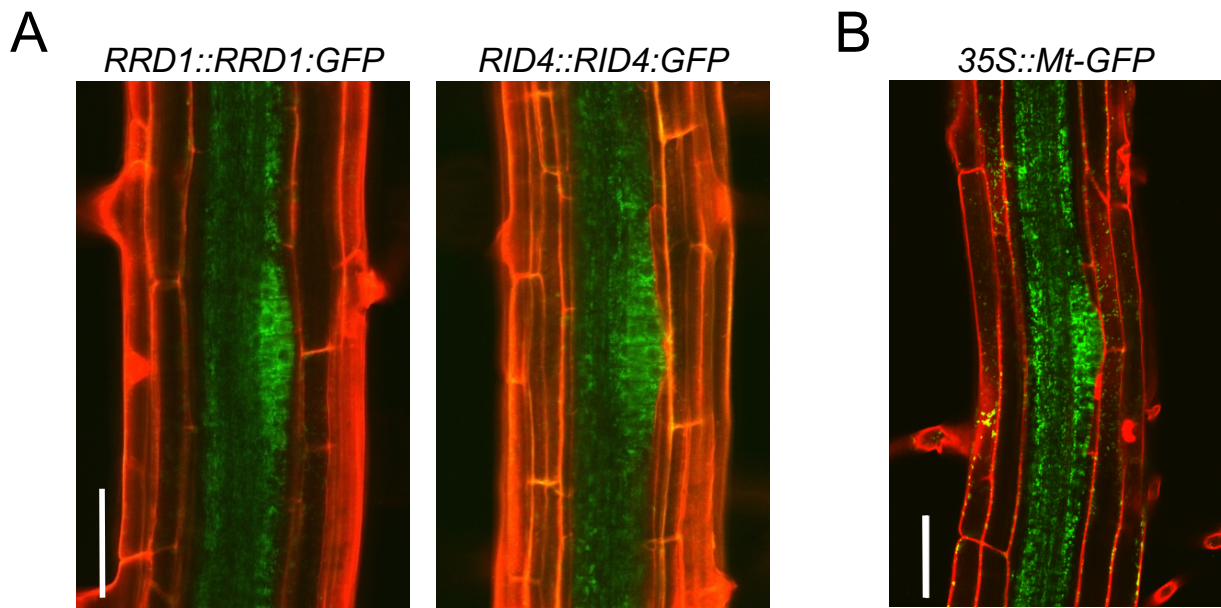


Fig. 19 The expression patterns of *RRD1* and *RID4* in the root.

Expression of *RRD1::RRD1:GFP* (A, left), *RID4::RID4:GFP* (A, right), and *35S::Mt-GFP* (B) at stage II of LR primordium development. 6-day old seedlings were used for the analysis. Propidium iodide was used as a red counterstain. Scale bars, 50 μm .

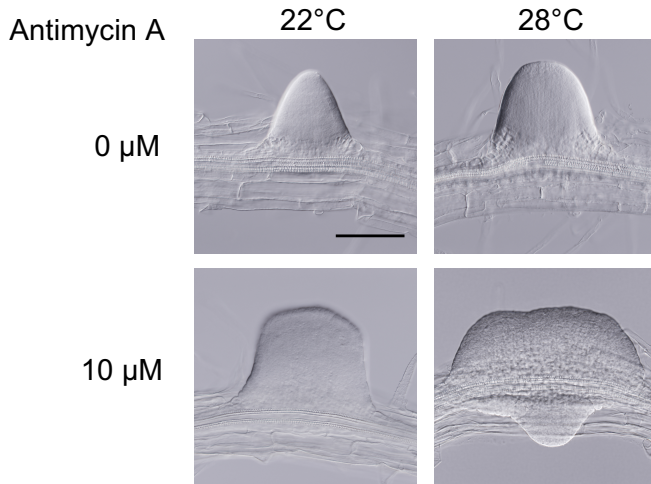
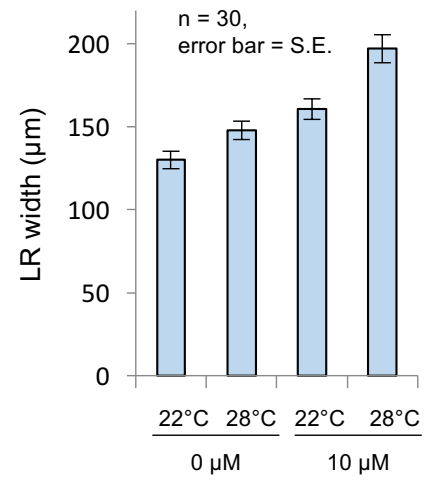
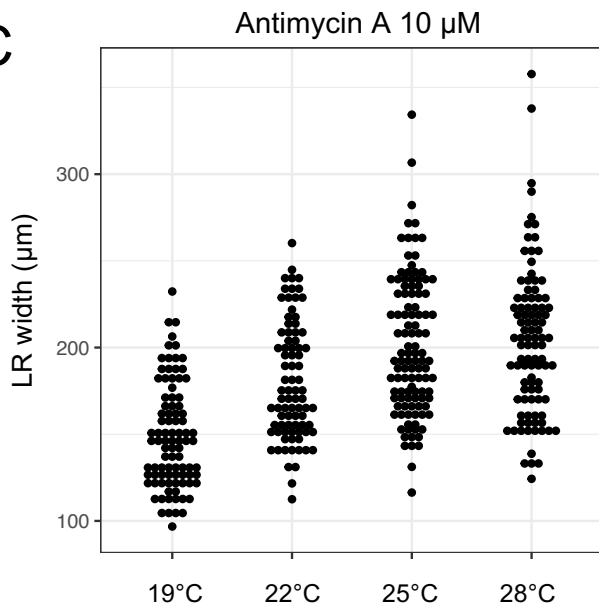
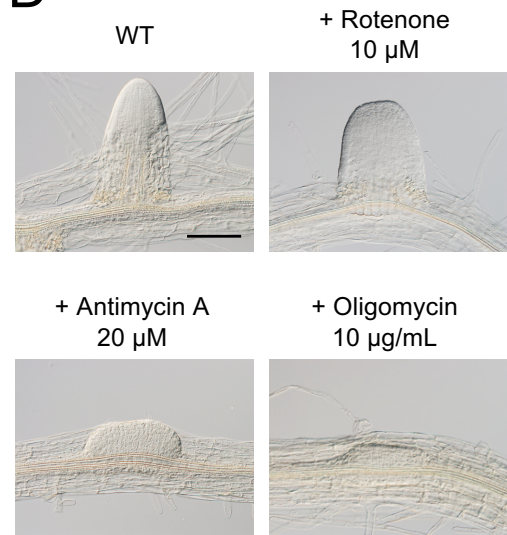
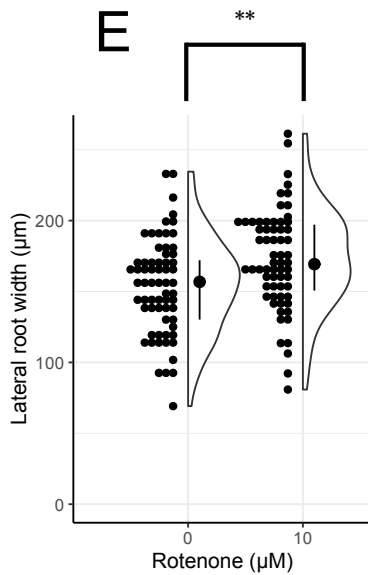
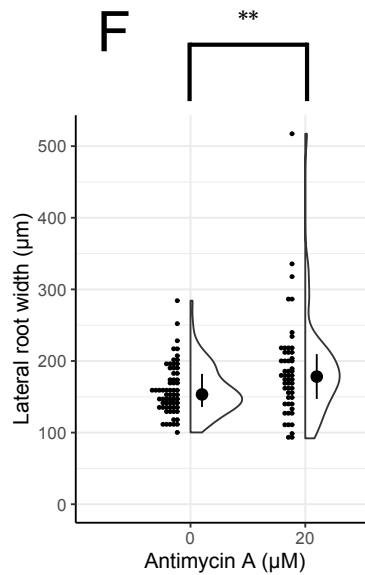
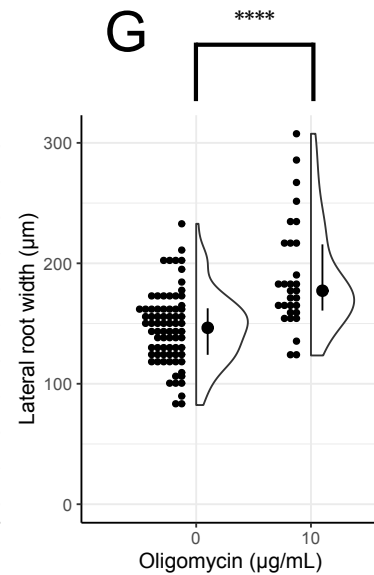
A**B****C****D****E****F****G**

Fig. 20 The effects of respiratory inhibitors on LR development

(A–C) LRs were induced from the wild-type in the presence of antimycin A at different temperatures (22°C and 28°C), and the basal width of the LRs that were formed was scored after 6 days in culture. (D–G) LRs were induced at 28°C from the wild-type (WT) plant in the presence of rotenone (E), antimycin A (F), or oligomycin (G), and the basal width of the LRs that were formed was scored after 6 days in culture (median, 25%–75% quantile, N = 30–76, * $P < 0.05$, ** $P < 0.01$, **** $P < 0.0001$, Mann–Whitney–Wilcoxon test). Typical LRs that were formed in each treatment are shown in (D). Scale bars, 100 μm .

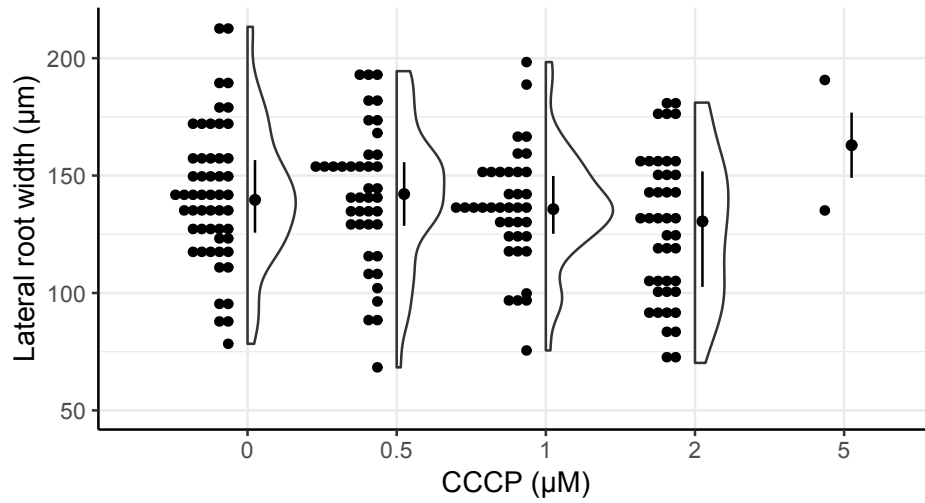
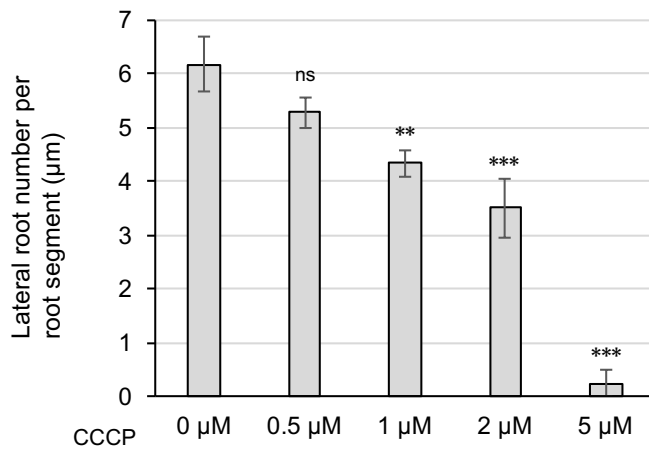
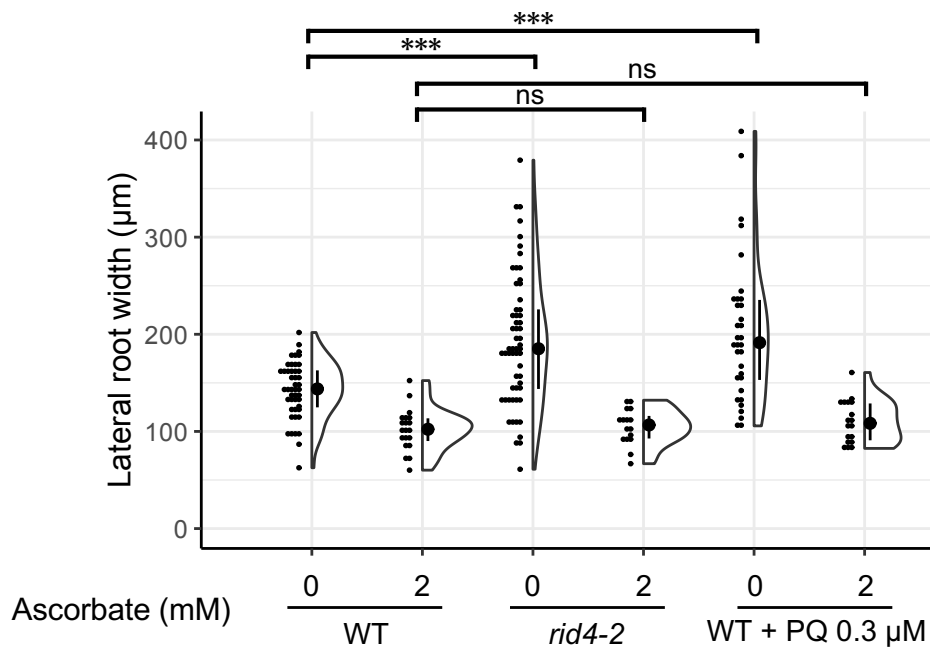
A**B**

Fig. 21 The effects of uncoupler CCCP on LR development

LRs were induced from the WT plant in the presence of CCCP. The basal width of LRs (A, median, 25%–75% quantile, N = 2–53, $P > 0.1$, Kruskal-Wallis test) and the number of LRs per segment (B, Number of segments = 12, $**P < 0.01$, $***P < 0.001$, Dunnett's test) were scored on the 6th day.

A



B

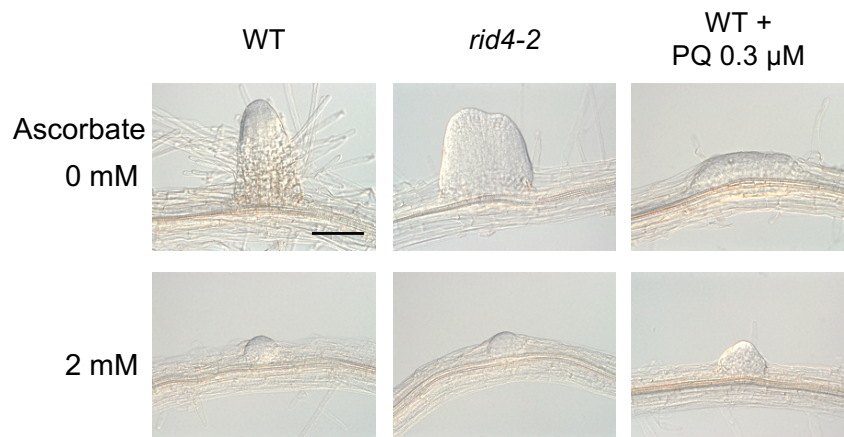


Fig. 22 The effects of the application of ascorbate on WT, PQ-treated, or *rid4-2* segments during LR formation.

(A) The basal width of the LRs formed was measured on the 6th day of LR induction (median, 25%–75% quantile, N = 16–58, *** $P < 0.001$, Mann–Whitney–Wilcoxon test with Bonferroni correction). (B) Representative images of LRs in each condition are shown. Scale bar, 100 µm.



Fig. 23 The effects of PQ and NPA on LR formation

Representative images of root explants cultured for 6 days in RIM containing NPA or PQ. Scale bar, 1 mm.



Fig. 24 The pattern of auxin response upon treatment with NPA or PQ

DR5::GUS expression at 12 hours after LR induction under treatment with NPA or PQ. Scale bar, 1 mm.

Fig.25 については5年以内に雑誌等で刊行予定のため、非公開。

E. Primers for amplifying cDNA of mitochondrial genes

Gene	Product size	Forward primer name	Forward primer sequence	Reverse primer name	Reverse primer sequence
atp1	1507	atp1Fw1	AGCTGCGGAACTAACGAATCTATTCGA	atp1Rv1	CTAAATTAAGCTAAAGCTCTTTCTTTTAAGA
atp4	489	atp4Fw1	GCTGCTATTCTATCTATTTGTGCATTAAGTTTCA	atp4Rv1	CTCTCGAATGAATTTCTACTCTTTC
atp6	857	atp6Fw1	AAGTGTGAGGCATTAACGCA	atp6Rv1	CCTAATTCAGACCCGGTTAATGCA
atp9	257	atp9Fw1	ATGACAAAGCGTGAGTATAAATCTC	atp9Rv1	CAGAATACGAATAAGATCAAAAAGGCCA
ccb2	621	ccb2Fw	CAGCCTTGAAGTGAATGAATT	ccb2Rv	TTAATCTTGTAATACTAATCGAGACC
ccb3	740	ccb3Fw	CTACGCGCAAATTCATTGG	ccb3Rv	GAGCGAGTGAAGTGGTTTTGGTA
ccb6c	1350	ccb6cFw	GGTCCAACACTACATAACTTTTTCTT	ccb6cRv	ATTATGAACTCCACGGAACTTTCT
ccb6c	1356	ccb6cFw2	ATGGTCCAACACTACATAACTT	ccb6cRv2	TGCAATTATGAACTCCACGGAA
ccb6n-A	511	ccb6n-A Fw4	GCGCCGCTTTATCCTGAAAG	ccb6n-A Rv4	CAGGATAGCATTTTGCGCC
ccb6n-A	561	ccb6n-A Fw5	AAACAACCACGAGCGTTTGG	ccb6n-A Rv5	ATCTCGTGCCAGATGCAACA
ccb6n-A	205	ccb6n-A Fw1	ATGTCAATATCAATATATGAATCTTTCAT	ccb6n-A Rv7	AGAAAGGTGCATTAGCGGTT
ccb6n B	547	ccb6n-Bfw1	CGAAGCGTGTCTCGTAAT	ccb6n-Brv1	GAGTGACGTAGATGCACAAGA
cob	1136	cobFw1	GACTATAAGGAACCAACGAT	cobRv1	ATCAGTCTCATCCGTGTAAG
cox2	760	cox2Fw2	ATGATTGTTCTAAAATGGTTATT	cox2Rv1	TTAATTGATTGGATACCAGGAAACC
cox3	798	cox3Fw1	ATGATTGAATCTCAGAGGCATTC	cox3Rv1	TCATATACCTCCCAACCAATAG
matR	574	matR Fw2	GGTTGAAGTTTAGACCCTCAC	matR Rv2	ATGCTCTTAACGCTCCCCAC
matR	512	matR Fw3	CTTGTCATAGCTCAGGTCCGA	matR Rv3	TGTTGGGGAACCTGCAAGG
nad1	948	nad1Fw	CCAGCTGAAATAGCTTGAATAAT	nad1Rv	AAAGGTGACTAAAAGACCAGAAAC
nad1a	372	nad1aFw1	GTACATAGCTGTTCCAGCTGA	nad1aRv	CCCGCTATAATAATCCATAAACAC
nad1b	269	nad1bFw	TCGAAATATGCCTTTCTAGGAG	nad1bRv	TCTACATTATAGCCTGCAACT
nad1c	316	nad1cFw	TCTTCAATGGGGCTGCTCT	nad1cRv	AAGGAAGCCATTGAAAGGTG
nad2a	560	nad2aFw1	CAGAATTCGTTCCGGATCCTC	nad2aRv1	TATTCCAGAGGAAAATGCAC
nad2b	881	nad2bFw1	CTTCGATCAATAGCCAAAGA	nad2bRv1	GATATGAACTGAGTGCCATT
nad3	360	nad3Fw1	ATGATGTCAGAATTTGCACCAAT	nad3Rv	TTACTCCCAGTCCGAAGCAC
nad4	1482	nad4Fw4	GTTAGAACATTTCTGTGAATGCT	nad4Rv1	TGAAATTTGCCATGTTGCAC
nad4L	278	nad4LFw1	TGGATCTTATCAAATATTTACATTTTCT	nad4LRv1	TTCTACAGCAATAGTACCTC
nad5a	1425	nad5aFw3	TTTGCCCTGCTCGGTAGTTC	nad5aRv1	TTGGCCAAGTATCCTACAAAGAGAC
nad5c	497	nad5cFw2	CCAATTTTGGGCCAATTCC	nad5cRv1	GAAAGACGATCGATTATCTACCCA
nad6	618	nad6Fw1	ATGATACITTTCTGTTTTGTCGAGC	nad6Rv1	TTAGTAGATCGTGAGTGGTCA
nad7	1171	nad7Fw1	ATGACGACTAGGAAAAGGCA	nad7Rv1	CTCCAACACAATATCTTGAGTACC
nad9	523	nad9Fw1	ACTTTACCCAAGAAATGGGTC	nad9Rv1	GCTGTTCCCAAGGACTAGC
orf240	696	orf240Fw1	ATGCGTAGTAGCGTTCTAAGATCACT	orf240Rv1	CAACCAGGACCTTTGGACCTC
orfX	861	orfXFw1	AATCCTTCACTTTTAGCTTTGAATTACT	orfXRv1	TCATTGATAGTTACTTTGCCAGGT
rpl16	540	rpl16fw2	ATGTATTTAACATAAAAATCGATTATGCT	rpl16Rv1	TTACGACCACTGAACAACTTGGTTG
rpl2	1050	rpl2Fw1	ATGAGACCAGGGAGAGCAAG	rpl2Rv1	TCACACAGTGAATAAGGGCTTAGG
rpl5	558	rpl5Fw1	ATGTTTCCACTCAATTTTCATTACG	rpl5Rv1	TTACTGAGTTTCCCCCTCATC
rps12	378	rps12Fw1	ATGCCACGTTTAAATCAATTGA	rps12rv1	TCATATCGATTTGGTTTTTCTGCACCA
rps3	1665	rps3Fw2	ATGGCACGAAAAGGAAATCCGATT	rps3Rv2	ITCGTACGTTTCCGGATATAGCACGTC
rps4	1089	rps4Fw1	ATGTGGCTGCTTAAAAACTGAT	rps4Rv1	TTATATGTTTTGGCCACGTCC
rps7	283	rps7Fw1	TAATCAAACCTATGGTTGACGCC	rps7Rv1	CGATTGGTGAAGCCAGTCC
rps14 (ψ)	234	pseudorps14Fw1	ACGTAGATTGCTCGCGGCT	pseudorps14Rv1	TCGAGATGCTAATCCACGAA

Table 1 Primers used in this study

(continued on next page)

F. Primers for sequencing cDNA of mitochondrial genes

Gene	Primer name	Primer sequence	Gene	Primer name	Primer sequence
atp1	atp1Fw2	GCTCAGTTGAAAGCTATGAAACAAG	nad3	nad3Fw1	ATGATGTCAGAAATTTGCACCAAT
atp1	atp1Rv1	CTAAATTAAGCTAAAGCTCTTTCTTTAAGA	nad3	nad3Rv	TTACTCCCGATCCGAAGCAC
atp4	atp4Fw1	GCTGCTATTCTATCTATTTGTGCATTAAGTTCGA	nad4	nad4Fw1	AGTGGTCTTATTCTGTGTCCT
atp4	atp4Rv1	CTCTCGAATGAATTTCTACTCTTTC	nad4	nad4Fw2	AAGATCAAGGCAGCATATCAGT
atp6	atp6Fw2	GGGCTTGATTTTGGGCGAAG	nad4	nad4Fw3	CATTGCTTACTCCTCAGTAGCCATA
atp6	atp6Rv2	TAGTCCAAGCGAACCACCTT	nad4	nad4Fw4	GTTAGAACATTTCTGTGAATGCT
atp9	atp9Fw1	ATGACAAAGCGTGAGTATAAATCTC	nad4	nad4Rv1	TGAAATTTGCCATGTTGCAC
atp9	atp9Rv1	CAGAATACGAATAAGATCAAAAAGGCCA	nad4	nad4Rv2	AGATTTGGCCGTAGA
ccb2	ccb2Fw	CAGCCTTGAAGTGAATGAATT	nad4L	nad4L Fw1	TGGATCTTATCAAAATTTTACATTTTCT
ccb2	ccb2Rv	TTAATCTTGTAACCTAATCGAGACC	nad4L	nad4LRv1	TTCTACAGCAATAGTACCTC
ccb2	ccb2Fw1	ATGAGACGACTTTTTCTTGAAGTAT	nad5a	nad5aFw1	GCTCCATGGATCTCATCGGAA
ccb2	ccb2 Fw3	TGCTTGGCAAAGATCCTACTTC	nad5a	nad5a Rv2	GGATTTCCCAACAGCACCAATA
ccb2	ccb2 Fw5	CGTCGTAACGCCCTTAATGC	nad5c	nad5cFw3	GCTGGTCTTCGATCAAGTTT
ccb2	ccb2 Fw7	TCCAGCAGTGGTTGGAACAG	nad5c	nad5cRv1	GAAAGACCATCGATTATGTACCCA
ccb3	ccb3Fw	CTACGCGCAAATTTCTATTGG	nad7	nad7Fw1	ATGACGACTAGGAAAAGGCA
ccb3	ccb3 Fw3	TGGATGCTCGTTTGACCTC	nad7	nad7Fw2	ATCTGCCTCTTGGCTTATGT
ccb3	ccb3 Rv4	GAGGTCAAACGAGCATCCCA	nad7	nad7Rv2	CTCGTAATGGTACCTCGCAATTCA
ccb6c	ccb6cFw1	TCAGAGCAAGTCGCCTATT	nad9	nad9Fw1	ACTTTACCCAAGAAATGGGTC
ccb6c	ccb6cFw2	ATGGTCCAACCTACATAACTT	nad9	nad9Rv1	GCTGTTCCCAAGGACTAGC
ccb6c	ccb6cFw3	TTACATGGACCCACTTTTCATTC	orf240A	orf240Fw1	ATGCGTAGTAGCGTCTAAGATCACT
ccb6n-A	ccb6n-A Fw4	GCGCGCTTTATCTCGAAAG	orf240A	orf240Rv1	CAACCAGGACCTTTGGACCTC
ccb6n-A	ccb6n-A Fw5	AAACAACCACCAGCGTTTGG	orfX	orfXFw1	AATCCTTCACTTTTAGCTTTGAATTACT
ccb6n-A	ccb6n-A Rv5	ATCTCGTGCCAGATGCAACA	orfX	orfXFw2	TACTTGTGGGTGCAACATCAACA
ccb6n-A	ccb6n-A Rv7	AGAAAGGTGCATTAGCGGTT	orfX	orfXFw3	ACGGAGGCCCTTTTCGACATT
ccb6n-B	ccb6n-BfW1	CGAAGCGTGTCTGTTGTAAT	orfX	orfXRv2	TGTTCTCCATAGCAACTGGGG
ccb6n-B	ccb6n-Bv1	GAGTGACGTAGATGCACAAGA	rpl2	rpl2Fw1	ATGAGACCAGGGAGAGCAAG
ccb6n-B	ccb6nB Rv3	AGCATTTTCTACGGGATCCC	rpl2	rpl2Rv1	TCACACAGTGAATAAGGGCTTAGG
cob	cobRv1	AGGTGTGATCAGTCTCATCCGTGT	rpl5	rpl5Fw1	ATGTTTCCACTCAATTTTCAATTACG
cob	cob Fw4	AGGAACCAACGATTCTCTCTTCT	rpl5	rpl5Rv1	TTACTGAGTTTCCCCTCATC
cox2	cox2Fw1	CTTTACTCAATGGACGAGGTAG	rpl5	rpl5 Rv2	AGACATCCATGCCCTCGGAG
cox2	cox2Fw2	ATGATTGTTCTAAAATGGTTATT	rpl16	rpl16fW2	ATGTATTTAACCAAAAATCGATTATGCT
cox2	cox2Rv1	TTAATTGATTGGATACCCGAGAACC	rpl16	rpl16Rv1	TTACGACCACTGAACAACTTGGTTG
cox2	cox2Rv2	GTCATTGAGTATAAGAGAGCAAAA	rpl16	rpl16Rv	CGGTAATAGGGAGATCCGCC
cox3	cox3Fw1	ATGATTGAATCTCAGAGGCATTC	rps3	rps3Fw3	CGATCAGGCTCGACGACCG
cox3	cox3Rv1	TCATATACCTCCCACCAATAG	rps3	rps3Fw4	ACTAAGACCTTAATTGAGTCAGTCA
matR	matR Fw2	GGTTGAAGTTTAGACCGCTCAC	rps3	rps3Rv1	ATATACGGATTCCTCCACCCCTTT
matR	matR Fw3	CTTGCATAGCTCAGGTCGGA	rps3	rps3Rv3	CCCCGGATTTCTGTTTGTCT
nad1	nad1aFw1	GTACATAGCTGTTCCAGCTGA	rps4	rps4Fw2	CCCTATTCTTATCGAAGAGAAGGAA
nad1	nad1aRv	CCCCTATAATAATCCATAAACAC	rps4	rps4Rv1	TTATATGTTTTGGCCACGTCC
nad1	nad1Fw	CCAGCTGAAACTTTGGAATAAT	rps4	rps4Rv2	TTTAGTAGTAGGCGGCATCC
nad1	nad1bFw	TCGAAATATGCCTTTCTAGGAG	rps4	rps4Rv3	TGAAGTTCGTTTTGTTCTCTG
nad1	nad1bRv	TCTACATTATAGCCTGCAACT	rps7	rps7Fw1	TAATCAAACCTATGGTTGACGCC
nad1	nad1c Fw2	GTTCTTTCTAGGAGTTGGC	rps7	rps7Rv1	CGATTGGTGAAGCCAGTCC
nad1	nad1cRv	AAGGAAGCCATTGAAAGGTG	rps12	rps12Fw1	ATGCCACGTTAATCAATTGA
nad2	nad2aFw1	CAGAATTCGTTCCGGATCCTC	rps12	rps12rV1	TCATATCGATTGGGTTTTCTGCACCA
nad2	nad2aRv2	CATCGAAATGGTACCAGCCG	rps14 (φ)	pseudorps14Fw1	ACGTAGATTGCTCGCGGCT
nad2	nad2bFw1	CTTCGATCAATTAGCCAAGA	rps14 (φ)	pseudorps14Rv1	TCGAGATGCTAATCCACGAA
nad2	nad2bRv2	TTGACTTTCTGTTGGGCCA			

Table 1 Primers used in this study

Gene	Function	ID	Gene	Function	ID	Gene	Function	ID
nad3	complex I	244920_s_at	cox2	complex IV	244950_at	ccb382 (ccb6n-A)	cytC biogenesis	244912_at
nad4	complex I	244929_at	cox3	complex IV	263509_s_at	ccb452 (ccb6c)	cytC biogenesis	244951_s_at
nad4L	complex I	244902_at	atp1	complex V	265228_s_at	rpl2	Ribosome	265232_s_at
nad5	complex I	257337_at	atp4 (orf25)	complex V	244901_at	rpl5	Ribosome	266044_s_at
nad5C	complex I	257338_s_at	atp6	complex V	266012_s_at	rps3-rpl16	Ribosome	244944_s_at
nad6	complex I	244953_s_at	atp8 (orfB)	complex V	265230_s_at	rps4	Ribosome	266042_s_at
nad7	complex I	244925_at	atp9	complex V	257339_s_at	rps7	Ribosome	265238_s_at
nad9	complex I	244943_at	ccb203 (ccb6n-B)	cytC biogenesis	244919_at	rps12	Ribosome	263502_s_at
cob	complex III	266045_s_at	ccb206 (ccb2)	cytC biogenesis	244945_at	matR	Maturase	244926_s_at
cox1	complex IV	257333_at	ccb256 (ccb3)	cytC biogenesis	263510_s_at	orfX	Protein transport ?	244928_s_at

Table 2 Functionally characterized mitochondrial genes studied in the microarray analysis

The function and array element ID of the characterized mitochondrial genes in the GeneChip Arabidopsis Genome ATH1 Array are shown.